JOC Article
pubs.acs.org/joc

Syntheses and Properties of Two-Dimensional, Dicationic Nonlinear Optical Chromophores Based on Pyrazinyl Cores

Benjamin J. Coe,*[,†] John Fielden,[†] Simon P. Foxon,[†] Madeleine Helliwell,[†] Inge Asselberghs,[‡] Koen Clays,[‡] Kurt De Mey,[‡] and Bruce S. Brunschwig[§]

[†]*School of Chemistry, University of Manchester, Oxford Road, Manchester M13 9PL, United Kingdom,* [‡]*Department of Chemistry, University of Leuven, Celestijnenlaan 200D, B-3001 Leuven, Belgium, and* [§]*Molecular Materials Research Center, Beckman Institute, MC 139-74, California Institute of Technology, 1200 East California Boulevard, Pasadena, California 91125, United States*

b.coe@manchester.ac.uk

Received October 5, 2010

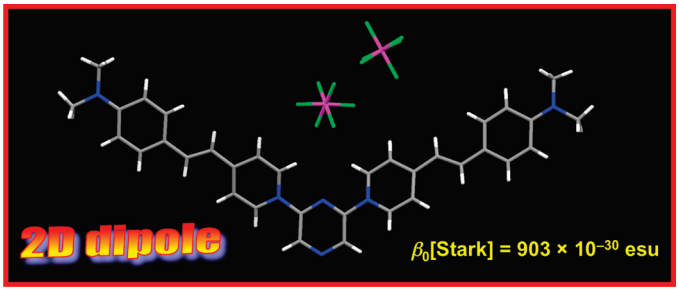

Six new dicationic 2D nonlinear optical (NLO) chromophores with pyrazinyl-pyridinium electron acceptors have been synthesized by nucleophilic substitutions of 2,6-dichloropyrazine with pyridyl derivatives. These compounds have been characterized as their PF_6^- salts by using various techniques including electronic absorption spectroscopy and cyclic voltammetry. Large red shifts in the intense, $\pi \rightarrow \pi^*$ intramolecular charge-transfer (ICT) transitions on replacing −OMe with $-NMe_2$ substituents arise from the stronger π-electron donor ability of the latter. Each compound shows a number of redox processes which are largely irreversible. Single crystal X-ray structures have been determined for five salts, including two nitrates, all of which adopt centrosymmetric packing arrangements. Molecular first hyperpolarizabilities β have been determined by using femtosecond hyper-Rayleigh scattering at 880 and 800 nm, and depolarization studies show that the NLO responses of the symmetric species are strongly 2D, with dominant "off-diagonal" β_{zyy} components. Stark (electroabsorption) spectroscopic measurements on the ICT bands afford estimated static first hyperpolarizabilities β_0. The directly and indirectly derived β values are large, and the Stark-derived β_0 response for one of the new salts is several times greater than that determined for (*E*)-4′-(dimethylamino)-*N*-methyl-4-stilbazolium hexafluorophosphate. These Stark spectroscopic studies also permit quantitative comparisons with related 2D, binuclear Ru^{II} ammine complex salts.

Introduction

Quaternized pyridine derivatives have attracted interest for many years and from various perspectives, including potential applications in electronic/optical devices.[1] Pyridinium species are readily synthesized, highly stable, and often combine intense visible absorptions (hence dye-like behavior) with reversible electrochemistry. Notable examples of recent reports involving such compounds include studies of aggregation-induced emission,[2] excited-state inclusion into zeolite channels,[3] multielectron redox,[4] ferroelectric organic−inorganic hybrid materials,[5] and

*To whom correspondence should be addressed. Fax 44 161-275-4598

(1) (a) Śliwa, W.; Matusiak, G.; Bachowska, B. *Croat. Chem. Acta* **2006**, *79*, 513–526. (b) Peltier, C.; Adamo, C.; Lainé, P. P.; Campagna, S.; Puntoriero, F.; Ciofini, I. *J. Phys. Chem. A* **2010**, *114*, 8434–8443.

(2) (a) Yuan, C.-X.; Tao, X.-T.; Ren, Y.; Li, Y.; Yang, J.-X.; Yu, W.-T.; Wang, L.; Jiang, M.-H. *J. Phys. Chem. C* **2007**, *111*, 12811–12816. (b) Yuan, C.-X.; Tao, X.-T.; Wang, L.; Yang, J.-X.; Jiang, M.-H. *J. Phys. Chem. C* **2009**, *113*, 6809–6814.

(3) Kim, H. S.; Pham, T. T.; Yoon, K. B. *J. Am. Chem. Soc.* **2008**, *130*, 2134–2135.

(4) Han, Z.-F.; Vaid, T. P.; Rheingold, A. L. *J. Org. Chem.* **2008**, *73*, 445–450.

Published on Web 11/16/2010 DOI: 10.1021/jo101966r

fluorescent probes for imaging of DNA in vivo.[6] Another important field that has proven very fruitful for exploitation of pyridinium salts is that of nonlinear optical (NLO) properties, relevant to applications ranging from advanced telecommunications to biological imaging.[7] In this context, particular attention has been paid to compounds such as (*E*)-4′-(dimethylamino)-*N*-methyl-4-stilbazolium tosylate (DAST)[8] and similar materials.[9] DAST crystals are now commercially available for THz wave generation via nonlinear frequency mixing,[10] useful for applications such as security scanning, biomedical analysis, and space communications.[11]

There are two major classes of molecular NLO effects. Quadratic (second-order) behavior originates from the first hyperpolarizability β that can lead to the susceptibility $\chi^{(2)}$ in bulk materials. In order for both β and $\chi^{(2)}$ to have nonzero values, the structure must lack centrosymmetry at the molecular and macroscopic levels. Second harmonic generation (SHG) and the linear electro-optic effect are the most commonly studied quadratic NLO phenomena. Cubic (third-order) behavior arises from the second hyperpolarizability γ, and its bulk counterpart, $\chi^{(3)}$, has nonzero values for any symmetry. Because this study involves measurements of only quadratic NLO effects, the remainder of this introduction concerns such properties exclusively.

Molecules that have large β values typically contain π-electron donor (π-ED) and acceptor (π-EA) groups linked via a polarizable π-system. In compounds such as DAST, a pyridinium ring acts as the π-EA. The β response is a third rank tensor that can possess a number of nonzero components. While the most heavily studied NLO molecules are simple 1D dipoles, multidimensional species such as 2D dipoles and 2D or 3D octupoles are also of great interest.[12,13] Chromophores of the

(5) Xu, G.; Li, Y.; Zhou, W.-W.; Wang, G.-J.; Long, X.-F.; Cai, L.-Z.; Wang, M.-S.; Guo, G.-C.; Huang, J.-S.; Bator, G.; Jakubas, R. *J. Mater. Chem.* **2009**, *19*, 2179–2183.

(6) Feng, S.-H.; Kim, Y. K.; Yang, S.-Q.; Chang, Y.-T. *Chem. Commun.* **2010**, *46*, 436–438.

(7) (a) *Molecular Nonlinear Optics: Materials, Physics and Devices*; Zyss, J. Academic Press: Boston, MA, 1994. (b) *Organic Nonlinear Optical Materials*; Bosshard, Ch., Sutter, K., Prêtre, Ph., Hulliger, J., Flörsheimer, M., Kaatz, P., Günter, P.; Advances in Nonlinear Optics, Vol. 1; Gordon & Breach: Amsterdam, The Netherlands, 1995. (c) *Nonlinear Optics of Organic Molecules and Polymers*; Nalwa, H. S., Miyata, S., Eds.; CRC Press: Boca Raton, FL, 1997. (d) Marder, S. R. *Chem. Commun.* **2006**, 131–134. (e) *Nonlinear Optical Properties of Matter: From Molecules to Condensed Phases*; Papadopoulos, M. G., Leszczynski, J., Sadlej, A. J., Eds.; Springer: Dordrecht, The Netherlands, 2006.

(8) Selected examples: (a) Marder, S. R.; Perry, J. W.; Schaefer, W. P. *Science* **1989**, *245*, 626–628. (b) Marder, S. R.; Perry, J. W.; Schaefer, W. P. *J. Mater. Chem.* **1992**, *2*, 985–986. (c) Marder, S. R.; Perry, J. W.; Yakymyshyn, C. P. *Chem. Mater.* **1994**, *6*, 1137–1147. (d) Lee, O.-K.; Kim, K.-S. *Photonics Sci. News* **1999**, *4*, 9–20. (e) Sohma, S.; Takahashi, H.; Taniuchi, T.; Ito, H. *Chem. Phys.* **1999**, *245*, 359–364. (f) Kaino, T.; Cai, B.; Takayama, K. *Adv. Funct. Mater.* **2002**, *12*, 599–603. (g) Mohan Kumar, R.; Rajan Babu, D.; Ravi, G.; Jayavel, R. *J. Cryst. Growth* **2003**, *250*, 113–117. (h) Geis, W.; Sinta, R.; Mowers, W.; Deneault, S. J.; Marchant, M. F.; Krohn, K. E.; Spector, S. J.; Calawa, D. R.; Lyszczarz, T. M. *Appl. Phys. Lett.* **2004**, *84*, 3729–3731. (i) Kuroyanagi, K.; Yanagi, K.; Sugita, A.; Hashimoto, H.; Takahashi, H.; Aoshima, S.-i.; Tsuchiya, Y. *J. Appl. Phys.* **2006**, *100*, 043117/1–043117/5. (j) Liu, J.-J.; Merkt, F. *Appl. Phys. Lett.* **2008**, *93*, 131105/1–131105/3. (k) Macchi, R.; Cariati, E.; Marinotto, D.; Roberto, D.; Tordin, E.; Ugo, R.; Bozio, R.; Cozzuol, M.; Pedron, D.; Mattei, G. *J. Mater. Chem.* **2010**, *20*, 1885–1890.

(9) Selected examples: (a) Yitzchaik, S.; Marks, T. J. *Acc. Chem. Res.* **1996**, *29*, 197–202. (b) Alain, V.; Blanchard-Desce, M.; Ledoux-Rak, I.; Zyss, J. *Chem. Commun.* **2000**, 353–354. (c) Cariati, E.; Ugo, R.; Cariati, F.; Roberto, D.; Masciocchi, N.; Galli, S.; Sironi, A. *Adv. Mater.* **2001**, *13*, 1665–1668. (d) Abbotto, A.; Beverina, L.; Bradamante, S.; Facchetti, A.; Klein, C.; Pagani, G. A.; Redi-Abshiro, M.; Wortmann, R. *Chem.−Eur. J.* **2003**, *9*, 1991–2007. (e) Kim, H. S.; Lee, S. M.; Ha, K.; Jung, C.; Lee, Y.-J.; Chun, Y. S.; Kim, D.; Rhee, B. K.; Yoon, K. B. *J. Am. Chem. Soc.* **2004**, *126*, 673–682. (f) Yang, Z.; Aravazhi, S.; Schneider, A.; Seiler, P.; Jazbinšek, M.; Günter, P. *Adv. Funct. Mater.* **2005**, *15*, 1072–1076. (g) Ruiz, B.; Yang, Z.; Gramlich, V.; Jazbinšek, M.; Günter, P. *J. Mater. Chem.* **2006**, *16*, 2839–2842. (h) Kim, H. S.; Sohn, K. W.; Jeon, Y.; Min, H.; Kim, D.; Yoon, K. B. *Adv. Mater.* **2007**, *19*, 260–263. (i) Yang, Z.; Jazbinšek, M.; Ruiz, B.; Aravazhi, S.; Gramlich, V.; Günter, P. *Chem. Mater.* **2007**, *19*, 3512–3518. (j) Morotti, T.; Calabrese, V.; Cavazzini, M.; Pedron, D.; Cozzuol, M.; Licciardello, A.; Tuccitto, N.; Quici, S. *Dalton Trans.* **2008**, 2974–2982. (k) Figi, H.; Mutter, L.; Hunziker, C.; Jazbinšek, M.; Günter, P.; Coe, B. J. *J. Opt. Soc. Am. B* **2008**, *25*, 1786–1793. (l) Compain, J.-D.; Mialane, P.; Dolbecq, A.; Marrot, J.; Proust, A.; Nakatani, K.; Yu, P.; Sécheresse, F. *Inorg. Chem.* **2009**, *48*, 6222–6228.

(10) Selected examples, see: (a) Kawase, K.; Mizuno, M.; Sohma, S.; Takahashi, H.; Taniuchi, T.; Urata, Y.; Wada, S.; Tashiro, H.; Ito, H. *Opt. Lett.* **1999**, *24*, 1065–1067. (b) Kawase, K.; Hatanaka, T.; Takahashi, H.; Nakamura, K.; Taniuchi, T.; Ito, H. *Opt. Lett.* **2000**, *25*, 1714–1716. (c) Taniuchi, T.; Okada, S.; Nakanishi, H. *Appl. Phys. Lett.* **2004**, *95*, 5984–5988. (d) Taniuchi, T.; Ikeda, S.; Okada, S.; Nakanishi, H. *Jpn. J. Appl. Phys.* **2005**, *44*, L652–L654. (e) Schneider, A.; Neis, M.; Stillhart, M.; Ruiz, B.; Khan, R. U. A.; Günter, P. *J. Opt. Soc. Am. B* **2006**, *23*, 1822–1835. (f) Schneider, A.; Stillhart, M.; Günter, P. *Opt. Express* **2006**, *14*, 5376–5384. (g) Yang, Z.; Mutter, L.; Stillhart, M.; Ruiz, B.; Aravazhi, S.; Jazbinšek, M.; Schneider, A.; Gramlich, V.; Günter, P. *Adv. Funct. Mater.* **2007**, *17*, 2018–2023.

(11) (a) *Terahertz Sources and Systems*; Miles, R. E., Harrison, P., Lippens, D., Eds.; NATO Science Series II, Vol. 27; Kluwer: Dordrecht, The Netherlands, 2001. (b) Ferguson, B.; Zhang, X.-C. *Nat. Mater.* **2002**, *1*, 26–33. (c) McEntee, J. *Chem. World* **2007**, March, 52−56. (d) http://www.teraview.com.

(12) Selected examples: (a) Wortmann, R.; Krämer, P.; Glania, C.; Lebus, S.; Detzer, N. *Chem. Phys.* **1993**, *173*, 99–108. (b) Moylan, C. R.; Ermer, S.; Lovejoy, S. M.; McComb, I.-H.; Leung, D. S.; Wortmann, R.; Krämer, P.; Twieg, R. J. *J. Am. Chem. Soc.* **1996**, *118*, 12950–12955. (c) Di Bella, S.; Fragalà, I.; Ledoux, I.; Diaz-Garcia, M. A.; Marks, T. J. *J. Am. Chem. Soc.* **1997**, *119*, 9550–9557. (d) Wolff, J. J.; Längle, D.; Hillenbrand, D.; Wortmann, R.; Matschiner, R.; Glania, C.; Krämer, P. *Adv. Mater.* **1997**, *9*, 138–143. (e) Averseng, F.; Lacroix, P. G.; Malfant, I.; Lenoble, G.; Cassoux, P.; Nakatani, K.; Maltey-Fanton, I.; Delaire, J. A.; Aukauloo, A. *Chem. Mater.* **1999**, *11*, 995–1002. (f) Hilton, A.; Renouard, T.; Maury, O.; Le Bozec, H.; Ledoux, I.; Zyss, J. *Chem. Commun.* **1999**, 2521–2522. (g) Lacroix, P. G. *Eur. J. Inorg. Chem.* **2001**, 339–348. (h) Ostroverkhov, V.; Petschek, R. G.; Singer, K. D.; Twieg, R. J. *Chem. Phys. Lett.* **2001**, *340*, 109–115. (i) Di Bella, S.; Fragalà, I.; Ledoux, I.; Zyss, J. *Chem.−Eur. J.* **2001**, *7*, 3738–3743. (j) Yang, M.-L.; Champagne, B. *J. Phys. Chem. A* **2003**, *107*, 3942–3951. (k) Wortmann, R.; Lebus-Henn, S.; Reis, H.; Papadopoulos, M. G. *J. Mol. Struct. (Theochem)* **2003**, *633*, 217–226. (l) Cui, Y.-Z.; Fang, Q.; Huang, Z.-L.; Xue, G.; Yu, W.-T.; Lei, H. *Opt. Mater.* **2005**, *27*, 1571–1575. (m) Rigamonti, L.; Demartin, F.; Forni, A.; Righetto, S.; Pasini, A. *Inorg. Chem.* **2006**, *45*, 10976–10989. (n) Li, H.-P.; Han, K.; Tang, G.; Shen, X.-P.; Wang, H.-T.; Huang, Z.-M.; Zhang, Z.-H.; Bai, L.; Wang, Z.-Y. *Chem. Phys. Lett.* **2007**, *444*, 80–84. (o) Zrig, S.; Koeckelberghs, G.; Verbiest, T.; Andrioletti, B.; Rose, E.; Persoons, A.; Asselberghs, I.; Clays, K. *J. Org. Chem.* **2007**, *72*, 5855–5858. (p) Liu, C.-G.; Qiu, Y.-Q.; Su, Z.-M.; Yang, G.-C.; Sun, S.-L. *J. Phys. Chem. C* **2008**, *112*, 7021–7028. (q) Li, H.-P.; Han, K.; Tang, G.; Li, M.-X.; Shen, X.-P.; Huang, Z.-M. *Mol. Phys.* **2009**, *107*, 1597–1603. (r) Muhammad, S.; Janjua, M. R. S. A.; Su, Z.-M. *J. Phys. Chem. C* **2009**, *113*, 12551–12557. (s) Sergeyev, S.; Didier, D.; Boitsov, V.; Teshome, A.; Asselberghs, I.; Clays, K.; Vande Velde, C. M. L.; Plaquet, A.; Champagne, B. *Chem.−Eur. J.* **2010**, *16*, 8181–8190.

(13) Selected examples: (a) Verbiest, T.; Clays, K.; Samyn, C.; Wolff, J.; Reinhoudt, D.; Persoons, A. *J. Am. Chem. Soc.* **1994**, *116*, 9320–9323. (b) Zyss, J.; Ledoux, I. *Chem. Rev.* **1994**, *94*, 77–105. (c) Dhenaut, C.; Ledoux, I.; Samuel, I. D. W.; Zyss, J.; Bourgault, M.; Le Bozec, H. *Nature* **1995**, *374*, 339–342. (d) McDonagh, A. M.; Humphrey, M. G.; Samoc, M.; Luther-Davies, B.; Houbrechts, S.; Wada, T.; Sasabe, H.; Persoons, A. *J. Am. Chem. Soc.* **1999**, *121*, 1405–1406. (e) Vance, F. W.; Hupp, J. T. *J. Am. Chem. Soc.* **1999**, *121*, 4047–4053. (f) Wolff, J. J.; Siegler, F.; Matschiner, R.; Wortmann, R. *Angew. Chem., Int. Ed.* **2000**, *39*, 1436–1439. (g) Cho, B. R.; Piao, M. J.; Son, K. H.; Lee, S. H.; Yoon, S. J.; Jeon, S.-J.; Cho, M.-H. *Chem.−Eur. J.* **2002**, *8*, 3907–3916. (h) Le Bouder, T.; Maury, O.; Bondon, O.; Costuas, K.; Amouyal, E.; Ledoux, I.; Zyss, J.; Le Bozec, H. *J. Am. Chem. Soc.* **2003**, *125*, 12284–12299. (i) Maury, O.; Viau, L.; Sénéchal, K.; Corre, B.; Guégan, J.-P.; Renouard, T.; Ledoux, I.; Zyss, J.; Le Bozec, H. *Chem.−Eur. J.* **2004**, *10*, 4454–4466. (j) Maury, O.; Le Bozec, H. *Acc. Chem. Res.* **2005**, *38*, 691–704. (k) Coe, B. J.; Harris, J. A.; Brunschwig, B. S.; Asselberghs, I.; Clays, K.; Garín, J.; Orduna, J. *J. Am. Chem. Soc.* **2005**, *127*, 13399–13410. (l) Le Floc'h, V.; Brasselet, S.; Zyss, J.; Cho, B. R.; Lee, S. H.; Jeon, S.-J.; Cho, M.-H.; Min, K. S.; Suh, M. P. *Adv. Mater.* **2005**, *17*, 196–200. (m) Hennrich, G.; Omenat, A.; Asselberghs, I.; Foerier, S.; Clays, K.; Verbiest, T.; Serrano, J. L. *Angew. Chem., Int. Ed.* **2006**, *45*, 4203–4206. (n) Jeong, M.-Y.; Kim, H. M.; Jeon, S.-J.; Brasselet, S.; Cho, B. R. *Adv. Mater.* **2007**, *19*, 2107–2111. (o) Liu, Y.; Xu, X.; Zheng, F.; Cui, Y. *Angew. Chem., Int. Ed.* **2008**, *47*, 4538–4541. (p) Akdas-Kilig, H.; Roisnel, T.; Ledoux, I.; Le Bozec, H. *New J. Chem.* **2009**, *33*, 1470–1473.

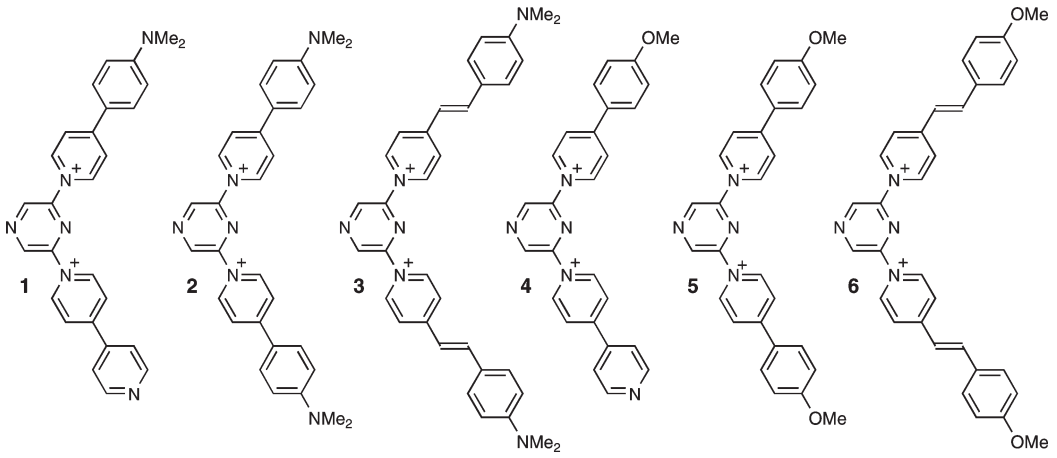

FIGURE 1. Chemical structures of the pyrazine derivatives prepared. Except for some of the X-ray crystal structure determinations, all of the measurements were made with PF_6^- salts.

latter types may offer significant potential advantages over 1D species, including enhanced NLO responses, without compromising visible transparency. In V-shaped molecules, the presence of more than one significant component of β can prevent reabsorption of SHG that is polarized perpendicular to the direction of the $\pi \rightarrow \pi^*$ intramolecular charge-transfer (ICT) transition dipole moment (μ_{12}); phase-matching between the fundamental and harmonic waves may also be facilitated.[12a]

Although current knowledge of pyridinium-based NLO compounds is very extensive, the vast majority of these materials contain methyl or alkyl quaternizing substituents. We have studied previously salts of chromophores containing *N*-arylpyridinium groups,[14] the enhanced electron accepting strength of which substantially increases static first hyperpolarizabilities β_0 when compared with more traditional *N*-alkylpyridinium compounds. Furthermore, SHG measurements on large single crystals of the salt (*E*)-4′-(dimethylamino)-*N*-phenyl-4-stilbazolium hexafluorophosphate afford a huge diagonal NLO susceptibility of $d_{111} \approx 290$ pm V^{-1} at 1907 nm (cf., DAST gives $d_{111} \approx 210$ pm V^{-1}).[15] Given that the *N*-(2-pyrimidyl)-pyridinium substituent is especially strongly electron-withdrawing, related species containing isomeric pyrazinyl groups are attractive. The precursor 2,6-dichloropyrazine has already been reacted with 4,4′-bipyridyl to create a ligand for copper(II) ions,[16] and provides an ideal foundation for the construction of 2D pyridinium chromophores. Here we describe a series of such new molecules that show promising quadratic NLO properties. Some related D_{3h} symmetric octupolar chromophores based on a 1,3,5-triazine core with stilbazolium substituents have been reported previously.[17]

Results and Discussion

Synthetic Studies. Six new chromophoric dications (Figure 1) have been synthesized via nucleophilic substitutions with 2,6-dichloropyrazine. **2**, **3**, **5**, and **6** were prepared by heating this precursor with 2 equiv of the appropriate 4-substituted pyridine in DMF at 120 °C, for up to 20 h. Purification was achieved by metathesis of the crude Cl^- salt to its PF_6^- counterpart, followed by reprecipitation from acetone/diethyl ether. Much lower yields (ca. 10%) are obtained for **3** and **6** than for **2** and **5** (up to 48%), perhaps because their ethenylene units make **3** and **6** vulnerable to decomposition under the relatively harsh reaction conditions used.

The asymmetric dications **1** and **4** were isolated as their PF_6^- salts in yields of ca. 20% by reacting 2,6-dichloropyrazine with mixtures of 4,4′-bipyridyl (4,4′-bpy) and the appropriate pyridine derivative. Because (*E*)-4-(4-methoxystyryl)-pyridine and (*E*)-4-(4-dimethylaminostyryl)pyridine are stronger nucleophiles than 4,4′-bpy, 1.5−2 equiv of the latter were used to favor formation of the target compounds. Nonetheless, substantial quantities of the bis-OMe or bis-NMe_2 products were still observed, with little or no formation of the bis-(4,4′-bpy) derivative. Using larger excesses of 4,4′-bpy did not give good results, presumably due to undesirable side reactions, while attempts to prepare monosubstituted derivatives from 2,6-dichloropyrazine yielded only the chromophores **2** and **5**, attributable to activation of the second chloride toward nucleophilic substitution by the presence of a nearby positive charge. The resulting product mixtures were separated by column chromatography on silica gel, eluting with aqueous KNO_3 in acetonitrile. This approach also allowed isolation of **1**, **2**, and **5** as their NO_3^- salts, leading to the crystal structures of [**1**][NO_3]$_2$ and [**5**][NO_3]$_2$ (see below). However, it was not possible to access pure [**4**][NO_3]$_2$ by this method because its high aqueous solubility precludes separation from the KNO_3 in the eluent. The identities and purities of the new compounds are confirmed by especially diagnostic ^{1}H NMR spectra together with ^{13}C NMR spectra, ESI$^+$-MS, and elemental analyses. The latter indicate that most of the PF_6^- salts retain small quantities of acetone, as confirmed by ^{1}H NMR spectroscopy. On the other hand, elemental analyses are consistent with hydration of the two

(14) (a) Coe, B. J.; Harris, J. A.; Asselberghs, I.; Clays, K.; Olbrechts, G.; Persoons, A.; Hupp, J. T.; Johnson, R. C.; Coles, S. J.; Hursthouse, M. B.; Nakatani, K. *Adv. Funct. Mater.* **2002**, *12*, 110–116. (b) Clays, K.; Coe, B. J. *Chem. Mater.* **2003**, *15*, 642–648. (c) Coe, B. J.; Harris, J. A.; Asselberghs, I.; Wostyn, K.; Clays, K.; Persoons, A.; Brunschwig, B. S.; Coles, S. J.; Gelbrich, T.; Light, M. E.; Hursthouse, M. B.; Nakatani, K. *Adv. Funct. Mater.* **2003**, *13*, 347–357. (d) Coe, B. J.; Harris, J. A.; Brunschwig, B. S.; Garín, J.; Orduna, J.; Coles, S. J.; Hursthouse, M. B. *J. Am. Chem. Soc.* **2004**, *126*, 10418–10427. (e) Coe, B. J.; Beljonne, D.; Vogel, H.; Garín, J.; Orduna, J. *J. Phys. Chem. A* **2005**, *109*, 10052–10057. (f) Coe, B. J.; Foxon, S. P.; Harper, E. C.; Harris, J. A.; Helliwell, M.; Raftery, J.; Asselberghs, I.; Clays, K.; Franz, E.; Brunschwig, B. S.; Fitch, A. G. *Dyes Pigm.* **2009**, *82*, 171–186.

(15) Figi, H.; Mutter, L.; Hunziker, C.; Jazbinšek, M.; Günter, P.; Coe, B. J. *J. Opt. Soc. Am. B* **2008**, *25*, 1786–1793.

(16) Sun, Y.-Q.; Zhang, J.; Chen, J.-L.; Yang, G.-Y. *Eur. J. Inorg. Chem.* **2004**, 3837–3841.

(17) (a) Cherioux, F.; Audebert, P.; Hapiot, P. *Chem. Mater.* **1998**, *10*, 1984–1989. (b) Brasselet, S.; Cherioux, F.; Audebert, P.; Zyss, J. *Chem. Mater.* **1999**, *11*, 1915–1920.

TABLE 1. Selected ^{1}H NMR Data for the Salts [1−6][PF$_6$]$_2$[a,b]

salt	$C_4H_2N_2$ singlets		C_5H_4N doublets						C_6H_4 doublets	
[**1**][PF$_6$]$_2$	10.02	10.00	10.16	9.57	9.04	8.95	8.57	8.14	8.25	7.02
[**2**][PF$_6$]$_2$	9.87		9.56	8.56					8.24	7.02
[**3**][PF$_6$]$_2$	9.83		9.53	8.32−8.26[c]					7.76	6.89
[**4**][PF$_6$]$_2$	10.10	10.09	10.13	9.87	9.04	8.95	8.84	8.15	8.34	7.29
[**5**][PF$_6$]$_2$	10.02		9.85	8.83					8.33	7.29
[**6**][PF$_6$]$_2$	9.96		9.76	8.55					7.86	7.12

[a]Recorded at 400 MHz in $(CD_3)_2CO$; all values are given in ppm with respect to TMS. [b]C_5H_4N and C_6H_4 signals distinguished by chemical shifts and coupling constants (ca. 7 Hz for C_5H_4N and ca. 9 Hz for C_6H_4), supported by ^{1}H COSY. [c]Signal overlaps with that for the ethenylene unit.

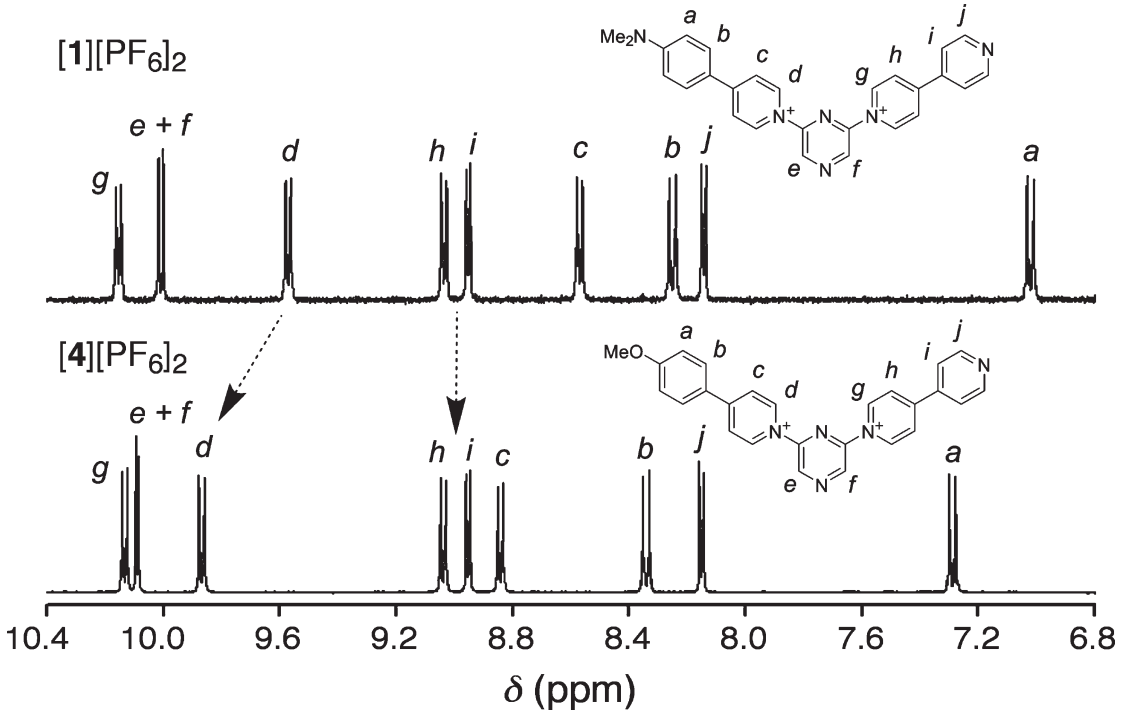

FIGURE 2. Aromatic regions of the ^{1}H NMR spectra of the salts [**1**][PF$_6$]$_2$ and [**4**][PF$_6$]$_2$ (400 MHz in $(CD_3)_2CO$ at 293 K). The arrows highlight the large shift in the 4-phenylpyridinium resonances on replacing $-NMe_2$ with $-OMe$ (e.g., environment *d*), and the contrasting lack of shifts in the 4,4′-bpy resonances (e.g., *h*, *i*).

NO_3^- salts. This observation is in keeping with the crystal structures of [**1**][NO_3]$_2$, and is also verified by TGA studies.

NMR Spectroscopy Studies. The chemical shifts and multiplicities for the aromatic protons are summarized in Table 1, their assignments being supported by ^{1}H COSY experiments with [**1**][PF$_6$]$_2$ and [**3**][PF$_6$]$_2$. Representative ^{1}H NMR spectra for [**1**][PF$_6$]$_2$ and [**4**][PF$_6$]$_2$ are shown in Figure 2. As expected, replacing a $-NMe_2$ group with the weaker π-ED $-OMe$ causes downfield shifts (Figure 2): up to ca. 0.3 ppm for the pyridyl (py) and phenyl proton signals, and up to ca. 0.15 ppm for the pyrazine (pyz) signals. The 4,4′-bpy signals show little change in moving from [**1**][PF$_6$]$_2$ to [**4**][PF$_6$]$_2$, indicating that electronic communication across the pyz ring is rather weak. Net shielding effects due to the mildly electron-donating ethenylene units, evidenced by upfield shifts in the range 0.03−0.48 ppm, are also observed on moving from **2** to **3** or from **5** to **6**.

While the ^{13}C NMR spectra are not quite as informative as their ^{1}H counterparts, they do provide further confirmation of the expected molecular structures. For the two asymmetric chromophores in [**1**/**4**][PF$_6$]$_2$, the total number of signals observed corresponds with the expected 18. The increased symmetry of the other species affords either 10 (for [**2**/**5**][PF$_6$]$_2$) or 12 C environments (for [**3**/**6**][PF$_6$]$_2$); all of the measured spectra agree with predictions, except for that of [**3**][PF$_6$]$_2$, which shows 11 resolved signals, presumably due to some coincidental overlap. In addition, the downfield shifts of the aryl/ethenylene signals evident in the ^{1}H spectra caused by replacing $-NMe_2$ with $-OMe$ are generally also observed in the ^{13}C spectra. For the pairs [**1**/**4**][PF$_6$]$_2$ and [**2**/**5**][PF$_6$]$_2$, the largest downfield shift (ca. 7.6−7.7 ppm) occurs for the signal found to lowest field, while for the pair [**3**/**6**][PF$_6$]$_2$, this signal shifts by only ca. 5.0 ppm. Several other signals show larger relative shifts of more than 8 ppm. However, it should also be noted that a few of the signals do show no significant change or even *upfield* shifts on replacing $-NMe_2$ with $-OMe$ (as much as ca. 5.7 ppm for one of the signals of [**1**/**4**][PF$_6$]$_2$).

Electronic Spectroscopy Studies. The UV−vis absorption spectra of salts [**1**−**6**][PF$_6$]$_2$ were recorded in acetonitrile and the results are presented in Table 2. Representative spectra of [**2**−**5**][PF$_6$]$_2$ are shown in Figure 3, while the others are included in the Supporting Information (Figures S1 and S2). In each case, the spectrum is dominated by a strong absorption band attributable to ICT transitions, with λ_{max} values in the range 490−600 nm for the $-NMe_2$-containing salts, and 370−450 nm for their $-OMe$ counterparts. Weaker absorptions due to other $\pi \rightarrow \pi^*$ transitions having

TABLE 2. UV−Vis Absorption and Electrochemical Data for Salts [1−6][PF$_6$]$_2$ in Acetonitrile[a]

salt	λ_{max}, nm (ε, 10^3 M^{-1} cm^{-1})[a]	E_{max} (eV)	assignment	E, V vs Ag−AgCl[b] E_{pa}, oxidations	E_{pc}, reductions
[**1**][PF$_6$]$_2$	493 (53.7)	2.52	ICT	1.37	−0.32[c]
	260 (25.5)	4.77	$\pi \rightarrow \pi^*$	1.24[d]	−0.78
[**2**][PF$_6$]$_2$	515 (82.1)	2.41	ICT	1.23[d]	−0.60
	263 (19.1)	4.71	$\pi \rightarrow \pi^*$		−0.77
[**3**][PF$_6$]$_2$	592 (82.9)	2.09	ICT	0.96	−0.52
	334 (17.7)	3.71	$\pi \rightarrow \pi^*$		−0.62
	280 (14.8)	4.43	$\pi \rightarrow \pi^*$		
[**4**][PF$_6$]$_2$	378 (36.2)	3.28	ICT		−0.32
	261 (20.6)	4.75	$\pi \rightarrow \pi^*$		−0.68
[**5**][PF$_6$]$_2$	393 (57.1)	3.16	ICT		−0.51
	270 (22.9)	4.59	$\pi \rightarrow \pi^*$		−0.71
[**6**][PF$_6$]$_2$	450 (63.1)	2.76	ICT		−0.43
	293 (17.6)[e]	4.23	$\pi \rightarrow \pi^*$		−0.57
	270 (17.8)[e]	4.59	$\pi \rightarrow \pi^*$		

[a]Solutions ca. $2-3 \times 10^{-5}$ M. [b]Solutions ca. 10^{-3} M in analyte and 0.1 M in [N(C$_4$H$_9$-*n*)$_4$]PF$_6$ at a 2 mm disk glassy carbon working electrode with a scan rate of 200 mV s^{-1}. Ferrocene internal reference $E_{1/2}$ = 0.44 V, ΔE_p = 70−90 mV. [c]A return wave at ca. −0.2 V is also observed for some samples. [d]A return wave at ca. 1.15 V is also observed for some samples. [e]Absorption is a poorly defined shoulder.

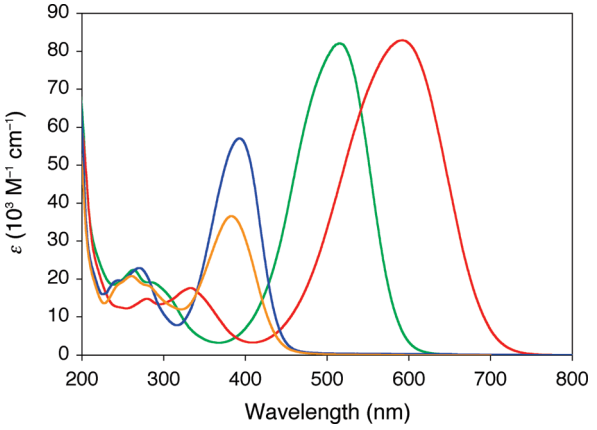

FIGURE 3. Electronic absorption spectra of [**2**][PF$_6$]$_2$ (green), [**3**][PF$_6$]$_2$ (red), [**4**][PF$_6$]$_2$ (orange), and [**5**][PF$_6$]$_2$ (blue) in acetonitrile at 293 K.

little or no directionality are also observed at shorter wavelengths.

The ICT absorptions for the −NMe$_2$ derivatives are markedly red-shifted and more intense when compared with those of their −OMe analogues (as shown for [**2**][PF$_6$]$_2$ and [**5**][PF$_6$]$_2$ in Figure 3). These differences are attributable to the stronger π-ED ability and more effective π-orbital overlap of the amino group. The decreases in E_{max} are ca. 0.7−0.8 eV, and the accompanying increases in ε are ca. 30−50%. Replacing a 4,4′-bpy unit with an π-ED-substituted biaryl fragment (**1** → **2** or **4** → **5**, Figure 3) also decreases E_{max} by ca. 0.1 eV and increases ε by over 50%. These enhanced intensities show that the overall extent of π-orbital overlap is greater when two π-ED groups are present, and this effect may also be responsible for the accompanying small red shifts observed. Inserting ethenylene units (**2** → **3** or **5** → **6**, Figure 3) decreases the ICT E_{max} by ca. 0.3−0.4 eV, but does not affect the band intensity significantly.

Electrochemical Studies. The salts [**1**−**6**][PF$_6$]$_2$ have been investigated by using cyclic voltammetry in acetonitrile, and the

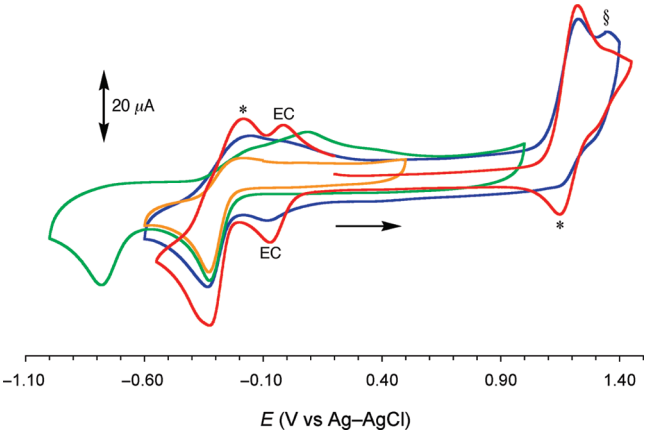

FIGURE 4. Cyclic voltammograms of [**1**][PF$_6$]$_2$ (200 mV s^{-1} in acetonitrile, glassy carbon working electrode). The single-headed arrow indicates the initial direction of the scans. The red trace starts from 0.2 V, and shows clearly an EC product wave, together with return peaks (∗) for both the first oxidation and first reduction process. The other traces start from −0.1 V and were obtained with a different sample. The orange trace shows no EC product waves, while the blue trace shows these appearing after oxidative scanning, and the second oxidation peak (§). The green trace shows both the first and second reduction peaks.

results are presented in Table 2. Representative voltammograms of [**1**][PF$_6$]$_2$ are shown in Figure 4. Although the related 2,6-bis(4-(pyridin-4-yl)pyridinium-1-yl)pyrazine dication has been described as showing two quasi-reversible reductions,[16] this term is actually inappropriate because the reverse waves are poorly defined. The new compounds show relatively complicated and generally irreversible electrochemical behavior, which is often influenced by the scan history and can vary between different analytically pure samples.

The −NMe$_2$ derivatives all show irreversible processes that can be ascribed to oxidations of the electron-rich fragments, with relatively weak return waves evident for some samples of [**1**][PF$_6$]$_2$ (Figure 4) and [**2**][PF$_6$]$_2$. Oxidation leads to the appearance of new waves to lower potentials, attributable to the products of EC reactions. In the case of [**1**][PF$_6$]$_2$, a second oxidation peak may also be detected at ca. 1.37 V. The E_{pa} values for initial oxidation of [**1**][PF$_6$]$_2$ and [**2**][PF$_6$]$_2$ are essentially identical, but the significantly lower value for [**3**][PF$_6$]$_2$ is consistent with the presence of electron-rich ethenylene units acting to destabilize the HOMO.

Two irreversible reductive processes are observed for all of these compounds, with some samples of [**1**][PF$_6$]$_2$ showing a return wave that appears to be associated with the first reduction (Figure 4). For the 4,4′-bpy-containing [**1**][PF$_6$]$_2$ and [**4**][PF$_6$]$_2$, the E_{pc} values for initial reduction are identical, but the second reduction peak for [**4**][PF$_6$]$_2$ is anodically shifted by 100 mV when compared with that of [**1**][PF$_6$]$_2$. This observation is consistent with the less electron-rich −OMe derivative being more readily reduced, i.e. relative stabilization of the LUMO in [**4**][PF$_6$]$_2$. For the symmetric chromophores, the E_{pc} values increase by 50−90 mV on replacing −NMe$_2$ with −OMe. However, given the accompanying increases in the ICT E_{max} values, evidently the relative stabilization of the HOMO in the −OMe derivatives greatly outweighs that of the LUMO. The addition of ethenylene units (**2** → **3** or **5** → **6**) also increases the E_{pc} values by 80−150 mV; the systems become more readily reduced due to

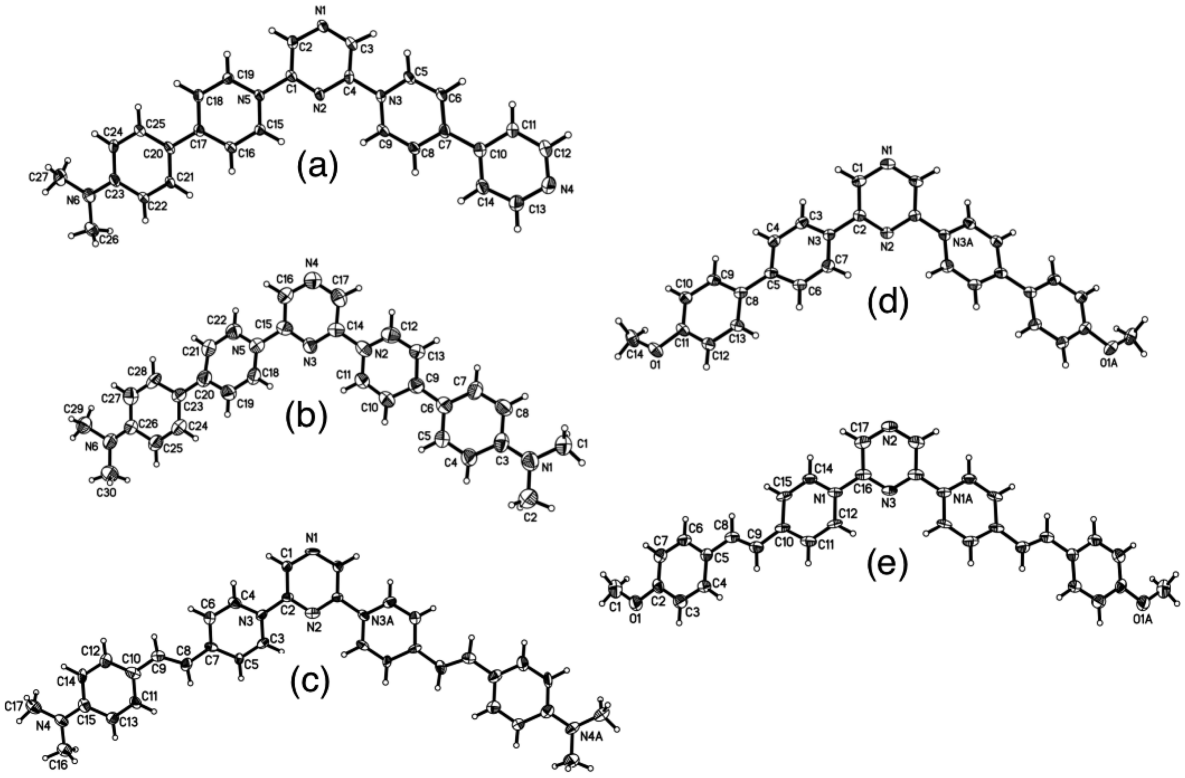

FIGURE 5. Representations of the molecular structures of the dications in the salts [**1**][NO_3]$_2$·2.5H_2O (a), [**2**][PF_6]$_2$ (b), [**3**][PF_6]$_2$·2Me_2CO (c), [**5**][NO_3]$_2$·2MeCN (d), and [**6**][PF_6]$_2$·MeCN (e) (50% probability ellipsoids).

TABLE 3. Twist Angles (deg) for the Salts [1][NO_3]$_2$·2.5H_2O, [2][PF_6]$_2$, [3][PF_6]$_2$·2Me_2CO, [5][NO_3]$_2$·2MeCN, and [6][PF_6]$_2$·MeCN

salt	py/pyz[a]	py/Ph[a]	py/py[a]	ethenylene/py[b]	ethenylene/Ph[b]	intrapyz[c]
[**1**][NO_3]$_2$·2.5H_2O	28.5, 34.1	11.4	18.3			3.0
[**2**][PF_6]$_2$	17.5, 20.8	14.6, 16.1				5.0
[**3**][PF_6]$_2$·2Me_2CO	14.9	9.5		0.7	7.6	2.1
[**5**][NO_3]$_2$·2MeCN	35.7	0.5				0.7
[**6**][PF_6]$_2$·MeCN	32.6	5.7		3.5	1.4	0.4

[a]Dihedral angle between the planes of the adjacent aryl rings (two values for lower symmetry structures). [b]Torsion angle between the ethenylene unit and the attached py or phenyl ring. [c]Twist angle between the two C−N−C subunits of the pyz ring. ESDs = ±(0.1−0.4)° for inter-ring and ethenylene/ring twists, ±(0.2−0.9)° for intra-pyz twists.

increased delocalization of the added electrons. Therefore, the decreases in the ICT energy gap on moving from **2** to **3** or from **5** to **6** can be attributed to both destabilization of the HOMO *and* stabilization of the LUMO. Replacing a 4,4′-bpy group with a π-ED-substituted biaryl unit (**1** → **2** or **4** → **5**) decreases the first E_{pc} value, since adding electrons becomes more difficult when the systems are more electron-rich.

X-ray Crystallographic Studies. X-ray crystal structures have been obtained for salts of all the new dications, except for [**4**]$^{2+}$. Several of the samples were small and weakly diffracting, but the data confirm the molecular structures and packing arrangements. Thermal ellipsoid plots of the five cations are shown in Figure 5.

In all cases, the C−NMe_2 or C−OMe distance is rather short for a formal single bond, ranging from 1.34(1) Å in [**2**][PF_6]$_2$ to 1.370(8) Å in [**5**][NO_3]$_2$·2MeCN, due to strong interactions between the lone pairs on the π-ED group and the phenyl ring. The extent of twisting in the dications is generally substantial (Table 3). Notably, the pyz rings show small departures from planarity in all of the −NMe_2-substituted species. It is likely that crystal packing effects, rather than electronic differences are responsible for the observed twists. Unfortunately, all of the salts crystallize centrosymmetrically, precluding bulk quadratic NLO activity. An absence of included solvent(s), observed here for only [**2**][PF_6]$_2$, would also be desirable for any materials-related applications. Despite being somewhat different at the molecular level, the salts [**5**][NO_3]$_2$·2MeCN and [**6**][PF_6]$_2$·MeCN both adopt the space group *Pnma*, with similar conformations and nearly identical packing arrangements (Figure 6).

In the −NMe_2-containing salts [**2**][PF_6]$_2$ and [**3**][PF_6]$_2$·2Me_2CO, centrosymmetric packing results from interspersed, directionally opposed lines of chromophoric dications running parallel/antiparallel to the crystallographic *c*-axis in [**2**][PF_6]$_2$ or the *b*-axis in [**3**][PF_6]$_2$·2Me_2CO. In [**1**][NO_3]$_2$·2.5H_2O, the ability of the free pyridyl N to accept H-bonds from water influences the extended structure. This pyridyl group connects [**1**]$^{2+}$ dications into an H-bonded network consisting of two formula units, i.e. two dications, four nitrate anions, and five water molecules (Figure 7); the overall structure is built by packing this motif. The H-bond distances lie in the range 2.521(4)−2.889(4) Å.

Hyper-Rayleigh Scattering Studies. The β values of salts [**1**−**6**][PF_6]$_2$ have been measured in acetonitrile solutions by

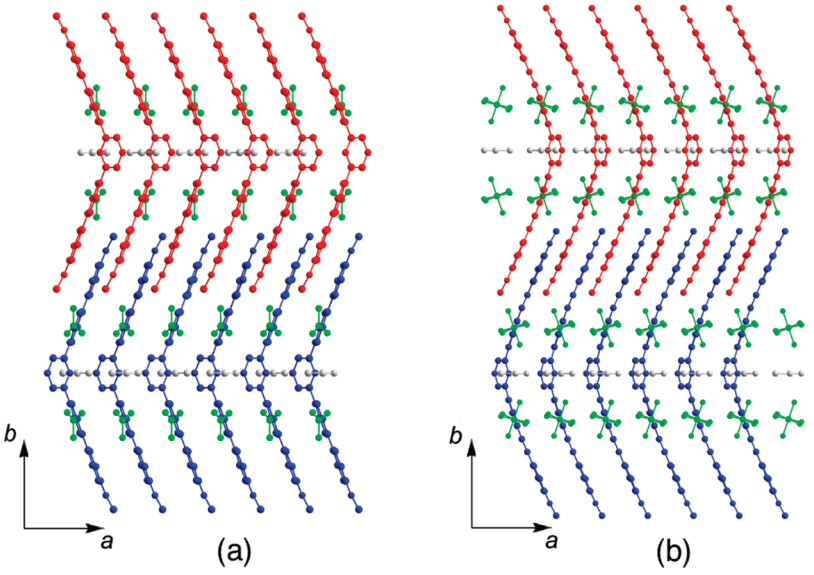

FIGURE 6. Crystal packing diagrams for (a) [**5**][NO_3]$_2$·2MeCN and (b) [**6**][PF_6]$_2$·MeCN viewed along the crystallographic *c*-axis. For clarity, directionally opposed lines of dications are colored red and blue, counteranions green, and acetonitrile molecules light gray.

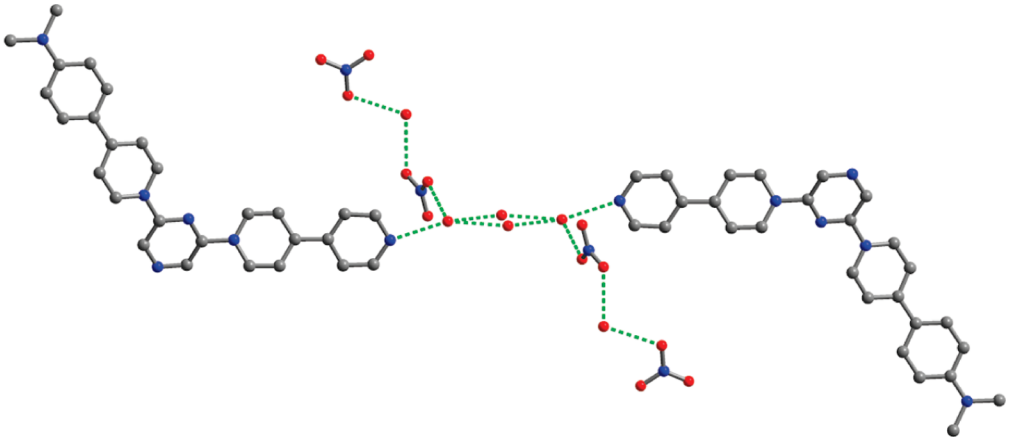

FIGURE 7. H-bonded dimer formed by two formula units of [**1**][NO_3]$_2$·2.5H_2O. Carbon is gray; N, blue; O, red; H, omitted; H-bonds represented as green dotted lines. The central water molecule is disordered over two 50% occupied, symmetry equivalent positions.

using the HRS technique[18,19] with a Ti^{3+}:sapphire laser and the results are shown in Table 4. All of the compounds were studied by using a fundamental wavelength of 800 nm, and data were also obtained for the relatively high-energy absorbers [**4**][PF_6]$_2$ and [**5**][PF_6]$_2$ by using 880 nm. However, salt [**6**][PF_6]$_2$ was not studied at the latter wavelength because its ICT maximum is very close to the second harmonic (SH) wavelength of 440 nm (Table 2). The hyperpolarizability data shown are orientationally averaged $\langle\beta_{HRS}^2\rangle^{1/2}$ values derived from the total HRS intensity, regardless of molecular symmetry. Because all of the new compounds show only a single low-energy ICT band, we have used the two-state model[20] and the λ_{max} values (Table 2) to derive estimated β_0 values; the results are included in Table 4.

The new chromophores, especially the symmetric ones, are not simple two-state systems, so the estimated β_0 values should be treated cautiously. Nevertheless, the $-NMe_2$ derivatives [**1**−**3**][PF_6]$_2$ do show a clear trend of increasing β_0 as the number of π-ED groups increases from 1 to 2 and also when inserting an ethenylene linkage; this is consistent with expectations based on the ICT energies (Table 2). While the β_0 values obtained with the 800 nm laser for two of the −OMe derivatives are strongly underestimated due to resonance, the data obtained with a 880 nm laser do show a small increase in β_0 on moving from [**4**][PF_6]$_2$ to [**5**][PF_6]$_2$.

Given their V-shaped molecular structures, the β responses of the dications **2**, **3**, **4**, and **6** are expected to be substantially 2D. A C_{2v} symmetric molecule has five nonzero components of the β tensor, β_{zzz}, β_{zyy}, β_{zxx}, β_{yyz}, and β_{xxz}.

(18) (a) Clays, K.; Persoons, A. *Phys. Rev. Lett.* **1991**, *66*, 2980–2983. (b) Clays, K.; Persoons, A. *Rev. Sci. Instrum.* **1992**, *63*, 3285–3289. (c) Hendrickx, E.; Clays, K.; Persoons, A. *Acc. Chem. Res.* **1998**, *31*, 675–683.

(19) (a) Olbrechts, G.; Strobbe, R.; Clays, K.; Persoons, A. *Rev. Sci. Instrum.* **1998**, *69*, 2233–2241. (b) Olbrechts, G.; Wostyn, K.; Clays, K.; Persoons, A. *Opt. Lett.* **1999**, *24*, 403–405. (c) Clays, K.; Wostyn, K.; Olbrechts, G.; Persoons, A.; Watanabe, A.; Nogi, K.; Duan, X.-M.; Okada, S.; Oikawa, H.; Nakanishi, H.; Vogel, H.; Beljonne, D.; Brédas, J.-L. *J. Opt. Soc. Am. B* **2000**, *17*, 256–265. (d) Franz, E.; Harper, E. C.; Coe, B. J.; Zahradnik, P.; Clays, K.; Asselberghs, I. *Proc. SPIE−Int. Soc. Opt. Eng.* **2008**, *6999*, 699923−1–699923−11.

(20) (a) Oudar, J. L.; Chemla, D. S. *J. Chem. Phys.* **1977**, *66*, 2664–2668. (b) Oudar, J. L. *J. Chem. Phys.* **1977**, *67*, 446–457.

TABLE 4. HRS Data and Depolarization Ratios for Salts [1−6][PF$_6$]$_2$ in Acetonitrile

	800 nm laser						880 nm laser					
	(10^{-30} esu)				(10^{-30} esu)		(10^{-30} esu)				(10^{-30} esu)	
salt	$\langle\beta_{HRS}^2\rangle^{1/2}$ [a]	β_0 [b]	ρ [c]	k	β_{zzz} [d]	β_{zyy} [d]	$\langle\beta_{HRS}^2\rangle^{1/2}$ [a]	β_0 [b]	ρ [c]	k	β_{zzz} [d]	β_{zyy} [d]
[**1**][PF$_6$]$_2$	126 ± 13	40 ± 4	3.7 ± 0.6		300 ± 31							
[**2**][PF$_6$]$_2$	265 ± 15	102 ± 6	2.4 ± 0.4	10	43 ± 6	430 ± 60						
[**3**][PF$_6$]$_2$	340 ± 25	183 ± 13	2.2 ± 0.3	10	55 ± 8	550 ± 80						
[**4**][PF$_6$]$_2$	290 ± 30	(24 ± 2)[e]					425 ± 15	90 ± 3	3.2 ± 0.5		1020 ± 150	
[**5**][PF$_6$]$_2$	550 ± 55	(14 ± 1)[e]					650 ± 30	105 ± 4	2.6 ± 0.4	10	105 ± 15	1050 ± 150
[**6**][PF$_6$]$_2$	570 ± 60	103 ± 11										

[a]Orientationally averaged β without any assumption of symmetry or contributing tensor elements, measured by using an 800 or 880 nm laser. The quoted cgs units (esu) can be converted into SI units ($C^3\ m^3\ J^{-2}$) by dividing by a factor of 2.693×10^{20}. [b]Static first hyperpolarizability estimated from $\langle\beta_{HRS}^2\rangle^{1/2}$ via the two-state model.[20] [c]Depolarization ratio. [d]β tensor components derived from the HRS intensity and depolarization ratio measurements by using eqs 1−3. [e]Underestimated due to proximity of ICT maximum to the SH wavelength at 400 nm.

Assuming Kleinman symmetry, $\beta_{zyy} = \beta_{yyz}$ and $\beta_{zxx} = \beta_{xxz}$, and if the structure is essentially 2D, then $\beta_{zxx} = \beta_{xxz} = 0$, so only β_{zzz} and β_{zyy} are significant. In order to derive "off-diagonal" tensor components, we have measured HRS depolarization ratios ρ for salts [**1**−**6**][PF$_6$]$_2$ and these are included in Table 4. The parameter ρ is the ratio of the intensities of the scattered SH light polarized parallel and perpendicular to the polarization direction of the fundamental beam.[21] A ρ value of 5 is the upper limit for purely dipolar symmetry, corresponding with a single tensor component β_{zzz}, under ideal experimental conditions. The octupolar reference compound crystal violet gives a much lower ρ value of 1.5.

The values of β_{zzz} and β_{zyy} can be determined from $\langle\beta_{HRS}^2\rangle$ and ρ as follows:

$$\begin{cases} \langle\beta_{HRS}^2\rangle = \langle\beta_{ZZZ}^2\rangle + \langle\beta_{YZZ}^2\rangle \\ \rho = \dfrac{\langle\beta_{ZZZ}^2\rangle}{\langle\beta_{YZZ}^2\rangle} \end{cases} \quad (1)$$

The HRS intensities with parallel polarization for fundamental and SH wavelengths, $\langle\beta_{ZZZ}^2\rangle$, and for perpendicular polarization, $\langle\beta_{YZZ}^2\rangle$, are given in terms of the molecular tensor components β_{zzz} and β_{zyy} according to

$$\begin{cases} \langle\beta_{ZZZ}^2\rangle = \dfrac{1}{7}\beta_{zzz}^2 + \dfrac{6}{35}\beta_{zzz}\beta_{zyy} + \dfrac{9}{35}\beta_{zyy}^2 \\ \langle\beta_{YZZ}^2\rangle = \dfrac{1}{35}\beta_{zzz}^2 - \dfrac{2}{105}\beta_{zzz}\beta_{zyy} + \dfrac{11}{105}\beta_{zyy}^2 \end{cases} \quad (2)$$

and ρ can be expressed in terms of the parameter $k = \beta_{zyy}/\beta_{zzz}$ by

$$\rho = \frac{15 + 18k + 27k^2}{3 - 2k + 11k^2} \quad (3)$$

The ρ values determined by using a 800 nm laser decrease on moving from [**1**][PF$_6$]$_2$ to [**2**][PF$_6$]$_2$, but are indistinguishable for [**2**][PF$_6$]$_2$ and [**3**][PF$_6$]$_2$. These observations are consistent with the more strongly 2D nature of the symmetric chromophores. In attempts to study the −OMe-containing compounds at 800 nm, very low concentrations were used in order to avoid reabsorption of the SH light. Under such conditions, the contribution of the solvent dominates over that of the solute, giving overestimated and meaningless ρ values. The ρ values determined at a fundamental wavelength of 880 nm appear to decrease on moving from [**4**][PF$_6$]$_2$ to [**5**][PF$_6$]$_2$, but the difference is within the experimental errors.

For the asymmetric compounds, [**1**][PF$_6$]$_2$ and [**4**][PF$_6$]$_2$, the relatively high ρ values indicate that the β_{zzz} tensor components dominate, so only these are reported. From an electronic/optical viewpoint, the dications **1** and **4** hence behave as essentially 1D dipoles, although they do still of course possess markedly 2D molecular structures. For the symmetric species, values of β_{zzz} and β_{zyy} have been derived by using eqs 1−3 (Table 4).[22] In all cases, β_{zyy} is dominant, as predicted by finite-field density functional theory (FF-DFT) calculations on V-shaped ruthenium complexes and disubstituted diquat derivatives.[23] However, it should be noted that ρ measurements can give misleading results, due to resonance effects and Kleinman symmetry breaking.[12h,24] Therefore, the quoted values of β_{zzz} and β_{zyy} for our new pyrazinyl species may be debatable, but the 2D nature of their β responses is not in doubt.

Stark Spectroscopic Studies. The salts [**1**−**6**][PF$_6$]$_2$ have been studied by using Stark spectroscopy[25,26] in butyronitrile glasses at 77 K and the results are presented in Table 5. Representative absorption and electroabsorption spectra are shown in Figure 8. For [**1**][PF$_6$]$_2$ and [**4**][PF$_6$]$_2$, the single visible absorption bands were fitted satisfactorily. However, Gaussian-fitting of the absorption spectra with three curves was required to successfully model the Stark data for the other compounds, due to the presence of clear shoulders to high energy of the absorption maxima. We have previously noted similar, but even more pronounced, changes in ICT spectra on moving from solutions at room temperature to frozen glasses containing

(21) Heesink, G. J. T.; Ruiter, A. G. T.; van Hulst, N. F.; Bölger, B. *Phys. Rev. Lett.* **1993**, *71*, 999–1002.

(22) It should be noted that eq 3 gives two solutions for k. However, because FF-DFT calculations on V-shaped ruthenium complexes and disubstituted diquat derivatives always predict dominance of β_{zyy} over β_{zzz} (see ref 23), we have chosen to use the positive k values that afford results consistent with these theoretical methods. In cases where eq 3 produces a solution of magnitude greater than 9, a value of 10 is used as an estimated upper limit for k; this approach stems from the nature of the mathematical relationship between k and ρ (see ref 41b).

(23) (a) Coe, B. J.; Harris, J. A.; Jones, L. A.; Brunschwig, B. S.; Song, K.; Clays, K.; Garín, J.; Orduna, J.; Coles, S. J.; Hursthouse, M. B. *J. Am. Chem. Soc.* **2005**, *127*, 4845–4859. (b) Coe, B. J.; Foxon, S. P.; Harper, E. C.; Helliwell, M.; Raftery, J.; Swanson, C. A.; Brunschwig, B. S.; Clays, K.; Franz, E.; Garín, J.; Orduna, J.; Horton, P. N.; Hursthouse, M. B. *J. Am. Chem. Soc.* **2010**, *132*, 1706–1723. (c) Coe, B. J.; Fielden, J.; Foxon, S. P.; Harris, J. A.; Helliwell, M.; Brunschwig, B. S.; Asselberghs, I.; Clays, K.; Garín, J.; Orduna, J. *J. Am. Chem. Soc.* **2010**, *132*, 10498–10512.

(24) Kaatz, P.; Shelton, D. P. *J. Chem. Phys.* **1996**, *105*, 3918–3929.

(25) (a) Shin, Y. K.; Brunschwig, B. S.; Creutz, C.; Sutin, N. *J. Phys. Chem.* **1996**, *100*, 8157–8169. (b) Coe, B. J.; Harris, J. A.; Brunschwig, B. S. *J. Phys. Chem. A* **2002**, *106*, 897–905.

(26) (a) Liptay, W. In *Excited States*,; Lim, E. C., Ed.; Academic Press: New York, 1974; Vol. 1, pp 129−229. (b) Bublitz, G. U.; Boxer, S. G. *Annu. Rev. Phys. Chem.* **1997**, *48*, 213–242. (c) Vance, F. W.; Williams, R. D.; Hupp, J. T. *Int. Rev. Phys. Chem.* **1998**, *17*, 307–329. (d) Brunschwig, B. S.; Creutz, C.; Sutin, N. *Coord. Chem. Rev.* **1998**, *177*, 61–79.

TABLE 5. ICT Absorption and Stark Spectroscopic Data for the Salts [1−6][PF$_6$]$_2$, [7]PF$_6$, [8]PF$_6$, [9][PF$_6$]$_6$, and [10][PF$_6$]$_6$

salt	ν_{max}[a] (cm^{-1})	λ_{max}[a] (nm)	E_{max}[a] (eV)	f_{os}[b]	μ_{12}[c] (D)	$\Delta\mu_{12}$[d] (D)	$\Delta\mu_{ab}$[e] (D)	r_{12}[f] (A)	r_{ab}[g] (A)	c_b^2[h]	H_{ab}[i] (10^3 cm^{-1})	β_0[j] (10^{-30} esu)	$\Sigma[\beta_0]$[k] (10^{-30} esu)
[**1**][PF$_6$]$_2$	19599	510	2.43	0.69	8.6	15.7	23.4	3.3	4.9	0.16	7.3	232	
[**2**][PF$_6$]$_2$	19180 (19029)	521 (526)	2.38 (2.36)	0.40	6.7	10.3	16.9	2.2	3.5	0.19	7.5	97	296
	(19800)	(505)	(2.45)	0.21	4.7	18.0	20.4	3.8	4.2	0.06	4.6	77	
	(20756)	(482)	(2.57)	0.55	7.5	12.3	19.4	2.6	4.0	0.18	8.1	122	
[**3**][PF$_6$]$_2$	16672 (16526)	600 (605)	2.07 (2.05)	0.56	8.5	11.7	20.6	2.4	4.3	0.22	6.8	234	903
	(17138)	(584)	(2.12)	0.21	5.1	21.5	23.7	4.5	4.9	0.05	3.6	142	
	(17855)	(560)	(2.21)	0.95	10.6	19.6	28.9	4.1	6.0	0.16	6.5	527	
[**4**][PF$_6$]$_2$	25406	394	3.15	0.44	6.1	14.0	18.5	2.9	3.9	0.12	8.3	61	
[**5**][PF$_6$]$_2$	24885 (24642)	402 (406)	3.08 (3.06)	0.28	4.9	10.5	14.4	2.2	3.0	0.13	8.4	32	104
	(25393)	(394)	(3.15)	0.25	4.5	11.1	14.4	2.3	3.0	0.11	8.1	27	
	(26618)	(376)	(3.30)	0.48	6.2	10.9	16.5	2.3	3.4	0.17	10.0	45	
[**6**][PF$_6$]$_2$	21393 (21275)	467 (470)	2.66 (2.64)	0.32	5.7	13.0	17.2	2.7	3.6	0.12	7.0	70	268
	(22389)	(447)	(2.78)	0.44	6.4	15.7	20.3	3.3	4.2	0.11	7.1	99	
	(23729)	(421)	(2.94)	0.51	6.8	16.1	21.0	3.3	4.4	0.12	7.7	99	
[**7**]PF$_6$[l]	20325	492	2.52	0.88	9.6	12.4	22.9	2.6	4.8	0.23	8.5	212	
[**8**]PF$_6$[l]	17762	563	2.20	0.76	9.5	14.5	23.9	3.0	5.0	0.20	7.1	318	
[**9**][PF$_6$]$_6$[m]	12663	790	1.57	0.51	9.3	16.3	24.7	3.4	5.2	0.17	4.8	662	
[**10**][PF$_6$]$_6$[m]	13469	742	1.67	0.63	10.0	19.4	27.9	4.0	5.8	0.15	4.8	816	

[a] In butyronitrile at 77 K; observed absorption maxima, maxima for Gaussian fitting functions for [**2**][PF$_6$]$_2$, [**3**][PF$_6$]$_2$, [**5**][PF$_6$]$_2$ and [**6**][PF$_6$]$_2$ in brackets. Data in all subsequent columns relate to fitted curves if used. [b] For [**1**][PF$_6$]$_2$, [**4**][PF$_6$]$_2$, [**7**]PF$_6$, [**8**]PF$_6$, [**9**][PF$_6$]$_6$ and [**10**][PF$_6$]$_6$, obtained from $(4.32 \times 10^{-9}$ M cm$^2)A$ where A is the numerically integrated area under the absorption peak; for [**2**][PF$_6$]$_2$, [**3**][PF$_6$]$_2$, [**5**][PF$_6$]$_2$ and [**6**][PF$_6$]$_2$, obtained from $(4.60 \times 10^{-9}$ M cm$^2)\varepsilon_{max} \times fw_{1/2}$ where ε_{max} is the maximal molar extinction coefficient and $fw_{1/2}$ is the full width at half height (in wavenumbers). [c] Calculated from eq 5. [d] Calculated from $f_{int}\Delta\mu_{12}$ using $f_{int} = 1.33$. [e] Calculated from eq 4. [f] Delocalized electron-transfer distance calculated from $\Delta\mu_{12}/e$. [g] Effective (localized) electron-transfer distance calculated from $\Delta\mu_{ab}/e$. [h] Calculated from eq 6. [i] Calculated from eq 7. [j] Calculated from eq 8. [k] Sum of the individual β_0 values (when using deconvolution). [l] Data taken from ref 14c. [m] Data taken from ref 28.

3-methylbenzothiazolium chromophores.[27] Such behavior may be attributable to the resolution of vibrational structure and/or electronically distinct ICT transitions at low temperatures.

The ICT bands of [**1**−**6**][PF$_6$]$_2$ show small red shifts on moving from acetonitrile solutions to butyronitrile glasses (Tables 2 and 5). The corresponding decreases in E_{max} lie in the range 0.02−0.13 eV, and are larger for the −OMe-substituted chromophores than for their $-NMe_2$ analogues. The E_{max} trends observed at room temperature are also found at 77 K, i.e. decreases on addition of ethylene bridges and increases on replacing $-NMe_2$ with −OMe. The trends in the band intensities at 77 K (i.e., f_{os} and μ_{12}) generally agree with those already noted for ε at room temperature (see above), but are more clearly apparent. When analyzing these data in cases involving spectral deconvolution, the total values are used. Replacing $-NMe_2$ with −OMe always decreases f_{os} and μ_{12}, while steady and substantial increases in both of these parameters occur on moving along the series **1**→**2**→**3** and **4**→**5**→**6**. The total increases in f_{os} and μ_{12} between the extremes are approximately 3-fold within both of these series.

Taking averaged values for the symmetric species, the quantities $\Delta\mu_{12}$, $\Delta\mu_{ab}$, r_{12}, and r_{ab} all show small decreases on replacing a 4,4′-bpy unit with an electron-donating fragment, but then increase somewhat on inserting ethenylene units. These trends are logical because these parameters relate directly to the chromophore length and π-ED−EA separation. For example, on moving from **2** to **1**, the overall distance over which the ICT process occurs should increase because the terminal pyridyl unit is weakly electron accepting. The other trend observed in these data is that replacing $-NMe_2$ with −OMe always decreases $\Delta\mu_{12}$, $\Delta\mu_{ab}$, r_{12}, and r_{ab}.

When analyzing the H_{ab} and c_b^2 data in cases involving spectral deconvolution, averages are used. The values of H_{ab} (the electronic coupling matrix element for the diabatic states) are all relatively large, indicating substantial π-coupling between the ED and EA groups. H_{ab} appears to be larger for the −OMe derivatives when compared with their $-NMe_2$ counterparts, but the differences may not be significant. The parameter c_b^2 reflects the extent of mixing between the diabatic states; this can reach a maximum possible value of 0.5, corresponding with essentially complete delocalization of the orbitals involved in the electronic excitation. The c_b^2 values for [**1**−**6**][PF$_6$]$_2$ lie in the range 0.11−0.16, indicating relatively limited delocalization and consistent with the description of the low-energy absorption bands as having substantial directionality, i.e. ICT character. The near constancy of c_b^2 shows that the extent of delocalization varies little among these chromophores.

Given that all of the visible absorptions are due to ICT excitations, even when using deconvolution, each component involves a ground and single excited state. Hence, the standard two-state model[20] (i.e., eq 8; see the Experimental Section) can be used to estimate β_0 values from the Stark data. The results are included in Table 5, and the sum totals of the β_0 responses associated with the three fitted Gaussian components are also quoted for the symmetric species. We have shown previously that using this approach typically gives total β_0 values similar to those obtained without spectral deconvolution.[14f,23b] The validity of applying such an additive two-state approach to multidimensional systems has been discussed in detail previously.[23c]

Two clear trends are evident in the estimated β_0 values. First, β_0 increases on moving along the series **1**→**2**→**3** and **4**→**5**→**6**. Enhancements of ca. 4-fold are observed on moving from **1** to **3** and from **4** to **6**. These increases arise from a combination of decreasing E_{max} and increasing μ_{12} and $\Delta\mu_{12}$ (Table 5). The smaller increases in β_0 on moving from **1** to **2** and from **4** to **5** are attributable to small decreases in E_{max} and increases in μ_{12}, with *counterbalancing decreases* in $\Delta\mu_{12}$. The second trend is that the β_0 values of the $-NMe_2$-substituted species are ca. 3−4-fold larger than those of their −OMe analogues. This effect largely results from the substantial accompanying decreases in E_{max}, but

(27) Coe, B. J.; Harris, J. A.; Hall, J. J.; Brunschwig, B. S.; Hung, S.-T.; Libaers, W.; Clays, K.; Coles, S. J.; Horton, P. N.; Light, M. E.; Hursthouse, M. B.; Garín, J.; Orduna, J. *Chem. Mater.* **2006**, *18*, 5907–5918.

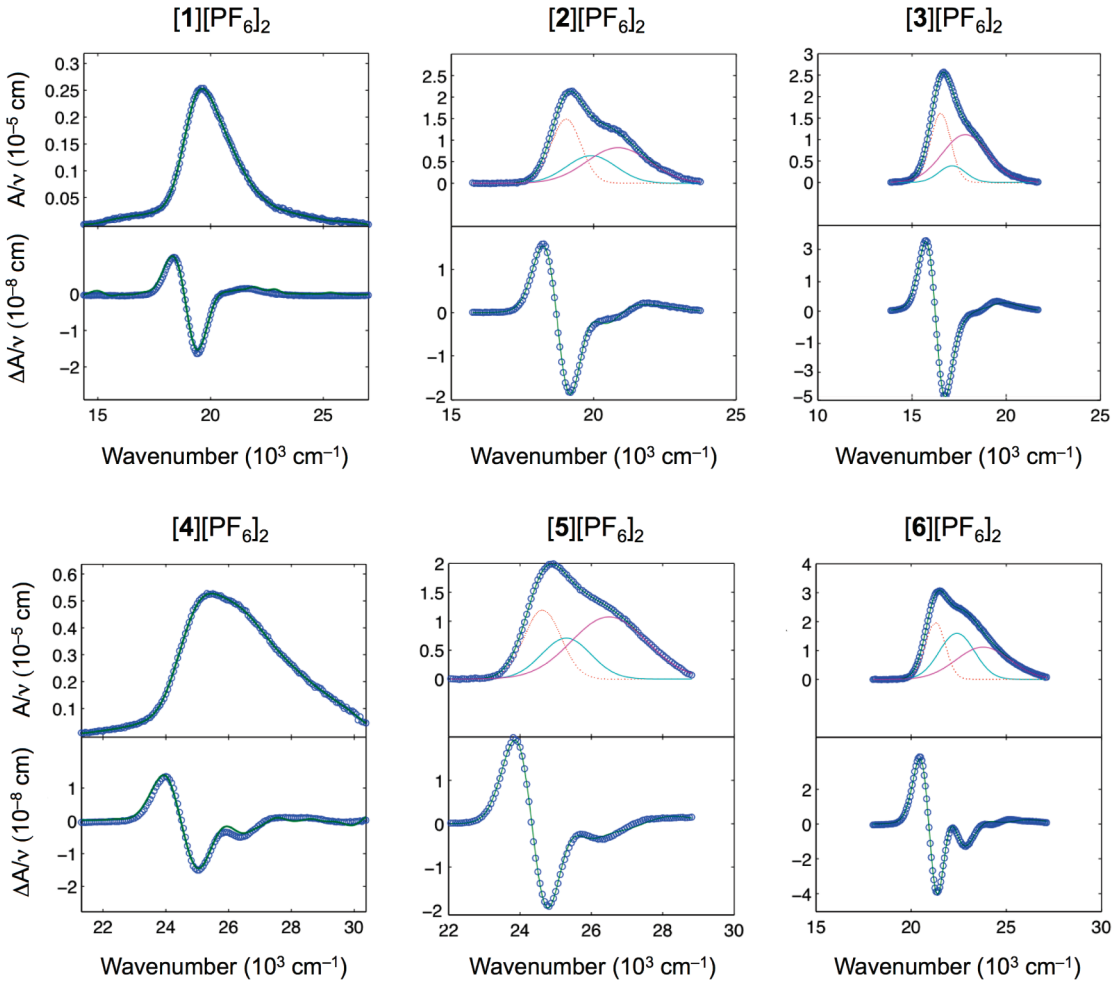

FIGURE 8. Stark spectra and calculated fits in an external electric field of 5.36×10^7 V m^{-1} for salts [**1**][PF$_6$]$_2$ and [**3**−**6**][PF$_6$]$_2$, and 4.39×10^7 V m^{-1} for [**2**][PF$_6$]$_2$. Top panels: Absorption spectrum showing Gaussian curves used in data fitting for [**2**][PF$_6$]$_2$, [**3**][PF$_6$]$_2$, [**5**][PF$_6$]$_2$, and [**6**][PF$_6$]$_2$. Bottom panels: Electroabsorption spectrum, experimental (blue), and fits (green) according to the Liptay equation.[26a]

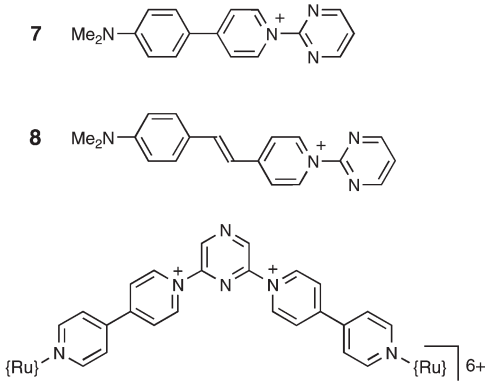

{Ru} = Ru^{II}(NH$_3$)$_5$ (**9**), *trans*-Ru^{II}(NH$_3$)$_4$(pyridine) (**10**)

FIGURE 9. Chemical structures of *N*-(2-pyrimidyl)pyridinium and Ru^{II} ammine complex chromophores, previously studied as their PF_6^- salts.[14c,28]

small increases in μ_{12} and $\Delta\mu_{12}$ also play some role. The total β_0 response of [**3**][PF$_6$]$_2$ is very large (ca. 900×10^{-30} esu) and considerably greater than that we obtained for [DAS]PF$_6$ by using the same approach previously (236×10^{-30} esu).[14c]

Given their structural similarities, comparisons with previously studied pseudolinear *N*-(2-pyrimidyl)pyridinium chromophores **7** and **8**,[14c] and also the dinuclear ruthenium(II) ammine complexes **9** and **10** (Figure 9)[28] are of interest. The complicating, highly variable effects of resonance in HRS studies mean that more useful comparisons are made by using the data obtained via Stark and associated measurements; those for [**7**]PF$_6$, [**8**]PF$_6$, [**9**][PF$_6$]$_6$, and [**10**][PF$_6$]$_6$ are hence included in Table 5. The visible absorption bands for the Ru^{II} ammine complex salts have metal-to-ligand charge-transfer character.

While the total β_0 value determined for [**2**]PF$_6$ is somewhat larger than that for [**7**]PF$_6$, the increase on moving from [**8**]PF$_6$ to [**3**]PF$_6$ is almost 3-fold. These enhanced NLO responses for the new 2D, pyrazinyl-based species are attributable primarily to the combined and pronounced effects of decreasing E_{max} and increasing μ_{12}, with the accompanying changes in $\Delta\mu_{12}$ being only slight (Table 5). The E_{max} values for the Ru^{II} ammine complex salts [**9**][PF$_6$]$_6$ and [**10**][PF$_6$]$_6$ are much lower than those of their purely organic counterparts with the same π-conjugation length, [**2**][PF$_6$]$_2$ and [**5**][PF$_6$]$_2$, showing that the pyridyl-coordinated metal centers are stronger π-ED groups when compared

(28) Coe, B. J.; Fielden, J.; Foxon, S. P.; Asselberghs, I.; Clays, K.; Brunschwig, B. S. *Inorg. Chem.* **2010**, *49*, 10718−10726.

with 4-(dimethylamino)phenyl or (especially) 4-methoxyphenyl fragments. The Ru^{II}-based chromophores show smaller values of f_{os} and μ_{12}, but larger dipole-moment changes and electron-transfer distances when compared with [**2**][PF_6]$_2$ and [**5**][PF_6]$_2$ (Table 5). The c_b^2 values are similar for all four related compounds, but H_{ab} is enhanced in the purely organic species. Most importantly, the β_0 responses for [**9**][PF_6]$_6$ and [**10**][PF_6]$_6$ are two or more times larger than that of [**2**][PF_6]$_2$. All of these comparative observations are generally in accord with our previous studies on pseudolinear chromophores,[14d,29] although the differences between the Ru^{II}-based and purely organic species are more pronounced in the new 2D systems. While the more highly conjugated chromophore in [**3**][PF_6]$_2$ has an estimated β_0 value possibly even larger than that of [**10**][PF_6]$_6$, the Ru^{II} pyridyl ammine analogues of [**3**][PF_6]$_2$ are not yet available for comparison.

As a final point, it should be noted that it is generally inappropriate to attempt to draw any direct comparisons between β_0 values determined via HRS and Stark spectroscopic measurements because these two techniques are applied under very different physical conditions. Further complicating factors, especially relevant to this study are the importance of resonance effects in HRS and the 2D nature of the chromophores (see above). Nonetheless, it is notable that our previous work with 1D Ru^{II} complexes shows that using the two-state eq 8 with Stark data can give excellent quantitative agreement with β_0 values derived from HRS experiments with a 1064 nm laser.[25b]

Conclusions

We have synthesized and characterized the first family of purely organic NLO chromophores based on pyrazinyl cores. Their UV−vis absorption spectra are dominated by intense ICT bands, with only one maximum observed in all cases at room temperature in acetonitrile. These absorptions show red shifts on inserting an ethenylene linkage and blue shifts on replacing $-NMe_2$ with $-OMe$ π-ED groups. Cyclic voltammograms show two or more redox processes, with a general lack of reversibility. Single-crystal X-ray structures have been determined for five salts, all of which pack centrosymmetrically. HRS studies with 800 or 880 nm laser wavelengths show relatively large β values, and depolarization measurements confirm the strongly 2D nature of the NLO responses for the symmetric compounds, with dominant β_{zyy} tensor components. Stark spectroscopy affords estimated β_0 values and shows that these increase with the number of π-ED groups and/or extending the π-conjugation, but decrease on replacing $-NMe_2$ with $-OMe$. The total β_0 response derived for the new salt [**3**][PF_6]$_2$ is several times larger than that determined for [DAS]PF_6 and closely related salts of 1D chromophores via the same indirect analytical approach. Complexes containing two pyridyl-coordinated Ru^{II} ammine π-ED groups show substantially larger β_0 responses when compared with their 4-(dimethylamino/methoxy)phenyl analogues with the same π-conjugation length, but [**3**][PF_6]$_2$ is possibly superior to even these metal-based species due to its extended π-system.

Experimental Section

Materials and Procedures. Acetonitrile was dried over CaH_2 and distilled under N_2, and dry DMF was purchased in SureSeal bottles. All other reagents and solvents were used as supplied. The compounds 4-(4-dimethylaminophenyl)pyridine,[30] 4-(4-methoxyphenyl)pyridine,[31] and (*E*)-4-(4-methoxystyryl)pyridine[32] were synthesized according to previously published methods. All reactions were carried out under an atmosphere of dry argon. Products were dried at room temperature overnight in a vacuum desiccator ($CaSO_4$) prior to characterization.

General Physical Measurements. All ^1H and ^{13}C NMR chemical shifts are quoted with respect to TMS. The fine splitting of pyridyl or phenyl ring AA′BB′ patterns is ignored and the signals are reported as simple doublets, with *J* values referring to the two most intense peaks. All mass spectra were recorded by using +electrospray. Cyclic voltammetric measurements were performed by using a single-compartment cell with a silver/silver chloride reference electrode (3 M NaCl, saturated AgCl) separated by a salt bridge from a 2 mm disk glassy carbon working electrode and Pt wire auxiliary electrode. Solutions containing ca. 10^{-3} M analyte and 0.1 M [$N(C_4H_9$-*n*$)_4$]PF_6 as the supporting electrolyte were deaerated by purging with N_2. All $E_{1/2}$ values were calculated from $(E_{pa} + E_{pc})/2$ at a scan rate of 200 mV s^{-1}.

Synthesis of 2-(4-(4-Dimethylaminophenyl)pyridinium-1-yl)-6-(4-(pyridin-4-yl)pyridinium-1-yl)pyrazine Hexafluorophosphate, [1][PF_6]$_2$. A mixture of 2,6-dichloropyrazine (75 mg, 0.503 mmol), 4-(4-dimethylaminophenyl)pyridine (75 mg, 0.378 mmol), and 4,4′-bipyridyl (120 mg, 0.768 mmol) in dry DMF (0.5 mL) was heated at 120 °C with stirring for 18 h. After cooling to room temperature, the mixture was washed out of the flask with ethanol (10 mL) and the crude chloride salts were precipitated by addition of diethyl ether. This mixture was purified by column chromatography on silica gel, eluting with 40:9:1−40:9:2 mixtures of acetonitrile/water/saturated aqueous KNO_3. The fractions containing **1** were combined, reduced in volume under vacuum, and recovered by precipitation with 10% aqueous NH_4PF_6. Final reprecipitation from acetone/diethyl ether yielded a deep red solid that was filtered off, washed with diethyl ether, and dried: 54 mg, 19%; δ_H (400 MHz, $(CD_3)_2CO$) 10.16 (2 H, d, J = 7.1 Hz, C_5H_4N), 10.02 (1 H, s, $C_4H_2N_2$), 10.00 (1 H, s, $C_4H_2N_2$), 9.57 (2 H, d, J = 7.3 Hz, C_5H_4N), 9.04 (2 H, d, J = 7.1 Hz, C_5H_4N), 8.95 (2 H, d, J = 6.1 Hz, C_5H_4N), 8.57 (2 H, d, J = 7.6 Hz, C_5H_4N), 8.25 (2 H, d, J = 9.3 Hz, C_6H_4), 8.14 (2 H, d, J = 6.3 Hz, C_5H_4N), 7.02 (2 H, d, J = 9.1 Hz, C_6H_4), 3.25 (6 H, s, 2Me). δ_C (100 MHz, $(CD_3)_2SO$) 156.6, 156.2, 154.4, 150.99, 150.96, 145.28, 145.25, 143.9, 141.0, 140.5, 140.2, 131.4, 125.6, 122.6, 119.8, 117.9, 112.7, 39.9 (Me, overlapped with solvent signal). Anal. Calcd (%) for $C_{27}H_{24}F_{12}N_6P_2 \cdot 0.25Me_2CO$: C, 45.23; H, 3.49; N, 11.40. Found: C, 45.57; H, 3.21; N, 11.76. *m*/*z* 577.6 ([M−PF_6]$^+$), 216.3 ([M − 2PF_6]$^{2+}$). Mp 210 °C dec. Note: substantial quantities of [**2**][PF_6]$_2$ (40 mg, 26%) were also obtained from this reaction.

Synthesis of 2,6-Bis(4-(4-dimethylaminophenyl)pyridinium-1-yl)-pyrazine Hexafluorophosphate, [2][PF_6]$_2$. A mixture of 2,6-dichloropyrazine (75 mg, 0.503 mmol) and 4-(4-dimethylaminophenyl)-pyridine (200 mg, 1.01 mmol) in dry DMF (0.7 mL) was heated at 120 °C with stirring for 20 h. After cooling to room temperature, the mixture was washed out of the flask with ethanol (10 mL) and the crude chloride salt was precipitated by addition of diethyl ether. This material was filtered off and redissolved in 50:50 methanol/water, then the product was precipitated by addition of 10% aqueous NH_4PF_6. Reprecipitation from acetone/diethyl ether yielded a deep red solid that was filtered off, washed with diethyl ether, and dried: 185 mg, 46%; δ_H (400 MHz, $(CD_3)_2CO$) 9.87 (2 H, s, $C_4H_2N_2$), 9.56 (4 H, d, J = 7.6 Hz, C_5H_4N), 8.56 (4 H, d, J = 7.6 Hz, C_5H_4N), 8.24 (4 H, d, J = 9.3 Hz, C_6H_4), 7.02 (4 H, d, J = 9.3 Hz, C_6H_4), 3.25 (12 H, s, 4Me). δ_C (100 MHz, $(CD_3)_2SO$) 156.5, 154.3, 145.1, 140.5, 139.3, 131.3, 119.8, 117.9, 112.6, 39.8

(29) Coe, B. J.; Harris, J. A.; Clays, K.; Persoons, A.; Wostyn, K.; Brunschwig, B. S. *Chem. Commun.* **2001**, 1548–1549.

(30) Vella, S. J.; Tiburcio, J.; Gauld, J. W.; Loeb, S. J. *Org. Lett.* **2006**, *8*, 3421–3424.

(31) Kitamura, Y.; Sako, S.; Udzu, T.; Tsutsui, A.; Maegawa, T.; Monguchi, Y.; Sajiki, H. *Chem. Commun.* **2007**, 5069–5071.

(32) Katritzky, A. R.; Short, D. J.; Boulton, A. J. *J. Chem. Soc.* **1960**, 1516–1518.

(Me, overlapped with solvent signal). Anal. Calcd (%) for $C_{30}H_{30}F_{12}N_6P_2 \cdot 0.6Me_2CO$: C, 47.78; H, 4.24; N, 10.51. Found: C, 47.97; H, 4.00; N, 10.49. *m/z* 619.1 ($[M - PF_6]^+$), 237.2 ($[M - 2PF_6]^{2+}$). Mp 250 °C dec (orange sublimate observed).

Synthesis of 2-(4-(4-Dimethylaminophenyl)pyridinium-1-yl)-6-(4-(pyridin-4-yl)pyridinium-1-yl)pyrazine Nitrate, [1][NO_3]$_2$, and 2,6-Bis(4-(4-dimethylaminophenyl)pyridinium-1-yl)pyrazine Nitrate, [2][NO_3]$_2$. These compounds were prepared by using the procedure described above for [**1**][PF_6]$_2$. After separation by column chromatography, [**1**][NO_3]$_2$ was recovered by removing acetonitrile under vacuum, followed by refrigeration. The red-brown solid was filtered off, washed with a small amount of cold water, and dried. [**2**][NO_3]$_2$ was precipitated by the addition of acetone, filtered off, washed with water, and dried to give a dark green solid. [**1**][NO_3]$_2$: 32 mg, 15%; δ_H (500 MHz, CD_3OD) 9.96 (2 H, d, J = 6.6 Hz, C_5H_4N), 9.82 (1 H, s, $C_4H_2N_2$), 9.78 (1 H, s, $C_4H_2N_2$), 9.38 (2 H, d, J = 6.6 Hz, C_5H_4N), 8.93 (2 H, d, J = 6.0 Hz, C_5H_4N), 8.89 (2 H, d, J = 6.6 Hz, C_5H_4N), 8.43 (2 H, d, J = 7.6 Hz, C_5H_4N), 8.20 (2 H, d, J = 9.1 Hz, C_6H_4), 8.15 (2 H, d, J = 6.3 Hz, C_5H_4N), 7.00 (2 H, d, J = 8.8 Hz, C_6H_4), 3.23 (6 H, s, 2Me). Anal. Calcd (%) for $C_{27}H_{24}N_8O_6 \cdot 1.5H_2O$: C, 55.57; H, 4.66; N, 19.20. Found: C, 55.25; H, 4.37; N, 18.92. *m/z* 216.2 ($[M - 2NO_3]^{2+}$). TGA: Calcd 4.63% H_2O for $C_{27}H_{24}N_8O_6 \cdot 1.5H_2O$; actual mass loss 4.30% by 168 °C. Mp 210−211 °C. [**2**][NO_3]$_2$: 32 mg, 27%; δ_H (500 MHz, CD_3OD) 9.65 (2 H, s, $C_4H_2N_2$), 9.35 (4 H, d, J = 7.3 Hz, C_5H_4N), 8.42 (4 H, d, J = 7.3 Hz, C_5H_4N), 8.18 (4 H, d, J = 9.1 Hz, C_6H_4), 7.00 (4 H, d, J = 9.3 Hz, C_6H_4), 3.23 (12 H, s, 4Me). Anal. Calcd (%) for $C_{30}H_{30}N_8O_6 \cdot 2H_2O$: C, 56.78; H, 5.40; N, 17.66. Found: C, 56.65; H, 5.24; N, 17.47. *m/z* 536.0 ($[M - NO_3]^+$). TGA: Calcd 5.67% H_2O for $C_{30}H_{30}N_8O_6 \cdot 2H_2O$; actual mass loss 5.72% by 97 °C and 6.08% by 224 °C (start of decomposition). Mp 243 °C dec (orange sublimate observed).

Synthesis of 2,6-Bis(4(2-(4-dimethylaminophenyl)-(*E*)-ethenyl)-pyridinium-1-yl)pyrazine Hexafluorophosphate, [3][PF_6]$_2$. A mixture of 2,6-dichloropyrazine (53 mg, 0.356 mmol) and (*E*)-4-[4-(dimethylamino)styryl]pyridine (171 mg, 0.762 mmol) in dry DMF (0.5 mL) was heated at 120 °C with stirring for 18 h. The reaction mixture was allowed to cool to room temperature before the deep purple solution was washed out of the flask with DMF (10 mL) and precipitated by addition of diethyl ether. The resulting crude, purple chloride salt was filtered off and redissolved in methanol and the product was precipitated by addition of 10% aqueous NH_4PF_6. Final reprecipitation from acetone/diethyl ether yielded a dark purple solid that was filtered off, washed with diethyl ether, and dried: 21 mg, 7%; δ_H (400 MHz, $(CD_3)_2CO$) 9.83 (2 H, s, $C_4H_2N_2$), 9.53 (4 H, d, J = 7.3 Hz, C_5H_4N), 8.32−8.26 (6 H, C_5H_4N + CH), 7.76 (4 H, d, J = 9.1 Hz, C_6H_4), 7.40 (2 H, d, J = 15.9 Hz, CH), 6.89 (4 H, d, J = 9.1 Hz, C_6H_4), 3.17 (12 H, s, 4Me). δ_C (125 MHz, $(CD_3)_2SO$) 157.2, 153.0, 146.9, 145.2, 140.3, 131.8, 122.6, 121.6, 116.8, 112.2, 39.8 (Me, overlapped with solvent signal). Anal. Calcd (%) for $C_{34}H_{34}F_{12}N_6P_2 \cdot 0.25Me_2CO$: C, 50.22; H, 4.31; N, 10.11. Found: C, 50.50; H, 4.12; N, 10.25. *m/z* 671.1 ($[M-PF_6]^+$), 263.5 ($[M-2PF_6]^{2+}$). Mp 200 °C dec.

Synthesis of 2-(4-(4-Methoxyphenyl)pyridinium-1-yl)-6-(4-(pyridin-4-yl)pyridinium-1-yl)pyrazine Hexafluorophosphate, [4][PF_6]$_2$. This compound was prepared and purified in a manner similar to [**1**][PF_6]$_2$ by using 4-(4-methoxyphenyl)pyridine (93 mg, 0.502 mmol) in place of 4-(4-dimethylaminophenyl)pyridine. The column was eluted with only 40:9:2 acetonitrile/water/saturated aqueous KNO_3, and a pale yellow solid was obtained: 60 mg, 17%; δ_H (400 MHz, $(CD_3)_2CO$) 10.13 (2 H, d, J = 7.3 Hz, C_5H_4N), 10.10 (1 H, s, $C_4H_2N_2$), 10.09 (1 H, s, $C_4H_2N_2$), 9.87 (2 H, d, J = 7.3 Hz, C_5H_4N), 9.04 (2 H, d, J = 7.3 Hz, C_5H_4N), 8.95 (2 H, d, J = 6.1 Hz, C_5H_4N), 8.84 (2 H, d, J = 7.6 Hz, C_5H_4N), 8.34 (2 H, d, J = 9.1 Hz, C_6H_4), 8.15 (2 H, d, J = 6.1 Hz, C_5H_4N), 7.29 (2 H, d, J = 9.1 Hz, C_6H_4), 4.00 (3 H, s, Me). δ_C (125 MHz, $(CD_3)_2SO$) 164.2, 157.8, 156.3, 151.2, 145.27, 145.25, 143.9, 142.5, 141.6, 141.3, 140.3, 131.4, 125.5, 124.7, 122.8, 122.4, 115.6, 56.0 (Me). Anal. Calcd (%) for $C_{26}H_{21}F_{12}N_5OP_2$: C, 44.02; H, 2.98; N, 9.87. Found: C, 43.66; H, 3.03; N, 10.09. *m/z* 209.6 ($[M - 2PF_6]^{2+}$). Mp 200 °C dec. Note: Substantial quantities of [**5**][PF_6]$_2$ (41 mg, 22%) were also obtained from this reaction.

Synthesis of 2,6-Bis(4-(4-methoxyphenyl)pyridinium-1-yl)pyrazine Hexafluorophosphate, [5][PF_6]$_2$. This compound was prepared and purified in a manner similar to [**2**][PF_6]$_2$ by using 2,6-dichloropyrazine (53 mg, 0.356 mmol) and 4-(4-methoxyphenyl)pyridine (135 mg, 0.729 mmol) in place of 4-(4-dimethylaminophenyl)-pyridine in dry DMF (0.5 mL) with a reaction time of 18 h. The crude product was washed out of the flask with DMF (10 mL), and a yellow solid was obtained: 90 mg, 34%; δ_H (400 MHz, $(CD_3)_2CO$) 10.02 (2 H, s, $C_4H_2N_2$), 9.85 (4 H, d, J = 7.3 Hz, C_5H_4N), 8.83 (4 H, d, J = 7.3 Hz, C_5H_4N), 8.33 (4 H, d, J = 8.8 Hz, C_6H_4), 7.29 (4 H, d, J = 8.8 Hz, C_6H_4), 4.00 (6 H, s, 2Me). δ_C (100 MHz, $(CD_3)_2SO$) 164.2, 157.7, 145.2, 142.5, 140.9, 131.4, 124.7, 122.8, 115.6, 56.0 (Me). Anal. Calcd (%) for $C_{28}H_{24}F_{12}N_4O_2P_2$: C, 45.54; H, 3.28; N, 7.59. Found: C, 45.67; H, 3.19; N, 7.49. *m/z* 593.4 ($[M - PF_6]^+$), 224.1 ($[M - 2PF_6]^{2+}$). Mp 215 °C dec.

Synthesis of 2-(4-(4-Methoxyphenyl)pyridinium-1-yl)-6-(4-(pyridin-4-yl)pyridinium-1-yl)pyrazine Nitrate, [5][NO_3]$_2$. This compound was obtained from the synthesis of [**4**][PF_6]$_2$ (see above) by evaporating the column fractions containing **5** until yellow crystals formed: 10 mg, 6.5%; δ_H (500 MHz, CD_3OD) 9.82 (2 H, s, $C_4H_2N_2$), 9.68 (4 H, d, J = 7.3 Hz, C_5H_4N), 8.69 (4 H, d, J = 6.9 Hz, C_5H_4N), 8.27 (4 H, d, J = 8.8 Hz, C_6H_4), 7.27 (4 H, d, J = 8.8 Hz, C_6H_4), 3.98 (6 H, s, 2Me). Anal. Calcd (%) for $C_{28}H_{24}N_6O_8 \cdot 1.1H_2O$: C, 56.77; H, 4.46; N, 14.18. Found: C, 56.34; H, 4.40; N, 14.67. *m/z* 510.2 ($[M - NO_3]^+$), 224.3 ($[M - 2NO_3]^{2+}$). TGA: Calcd 3.3% H_2O for $C_{28}H_{24}N_6O_8 \cdot 1.1H_2O$; actual mass loss of 3.05% by 208 °C. Mp 192−193 °C.

Synthesis of 2,6-Bis(4-(2-(4-methoxyphenyl)-(*E*)-ethenyl)pyridinium-1-yl)pyrazine Hexafluorophosphate, [6][PF_6]$_2$. This compound was prepared and purified in a manner similar to [**3**][PF_6]$_2$ by using (*E*)-4-(4-methoxystyryl)pyridine (152 mg, 0.719 mmol) in place of (*E*)-4-[4-(dimethylamino)styryl]pyridine, with a reaction time of 4 h. An orange solid was obtained: 35 mg, 12%; δ_H (400 MHz, $(CD_3)_2CO$) 9.96 (2 H, s, $C_4H_2N_2$), 9.76 (4 H, d, J = 6.3 Hz, C_5H_4N), 8.55 (4 H, d, J = 6.6 Hz, C_5H_4N), 8.34 (2 H, d, J = 16.1 Hz, CH), 7.86 (4 H, d, J = 8.8 Hz, C_6H_4), 7.64 (2 H, d, J = 16.1 Hz, CH), 7.12 (4 H, d, J = 9.1 Hz, C_6H_4), 3.92 (6 H, s, 2Me). δ_C (125 MHz, $(CD_3)_2SO$) 162.2, 157.4, 145.2, 144.9, 141.7, 140.2, 131.0, 127.7, 123.1, 120.8, 115.0, 55.6 (Me). Anal. Calcd (%) for $C_{32}H_{28}F_{12}N_4O_2P_2 \cdot 0.5Me_2CO$: C, 49.10; H, 3.81; N, 6.84. Found: C, 49.11; H, 3.53; N, 6.84. *m/z* 645.2 ($[M - PF_6]^+$), 250.1 ($[M - 2PF_6]^{2+}$). Mp 177 °C dec. Note: A similar reaction with a longer heating time of 18 h (as used for the other compounds) gave a lower yield of below 10%.

X-ray Crystallography. Crystal structures have been obtained for the salts [**1**][NO_3]$_2 \cdot 2.5H_2O$, [**2**][PF_6]$_2$, [**3**][PF_6]$_2 \cdot 2Me_2CO$, [**5**][NO_3]$_2 \cdot 2$MeCN, and [**6**][PF_6]$_2 \cdot$MeCN. Suitable crystals were grown by slow evaporation of an acetonitrile solution of [**1**][NO_3]$_2$, or by diffusion of diethyl ether vapor at room temperature into solutions of the salts [**2**][PF_6]$_2$/[**3**][PF_6]$_2$ in acetone, or [**5**][NO_3]$_2$/[**6**][PF_6]$_2$ in acetonitrile. Data were collected on Oxford Diffraction XCalibur 2 or Bruker APEX II CCD X-ray diffractometers with Mo Kα radiation (λ = 0.71073 Å), and the data were processed by using the Oxford Diffraction CrysAlis RED[33] or Bruker SAINT[34] and SADABS[35] software packages. The structures were solved by direct methods using SIR-92[36] via WinGX,[37] or SHELXS-97,[38]

(33) *CrysAlis RED*, Version 1.171.32.4; Oxford Diffraction Ltd.; Yarnton: Oxfordshire, United Kingdom, 2006.
(34) *SAINT*, Version 6.45, Bruker AXS Inc.; Madison: Wisconsin, 2003.
(35) *SADABS*, Version 2.10; Bruker AXS Inc.; Madison: Wisconsin, 2003.
(36) Altomare, A.; Cascarano, G.; Giacovazzo, C.; Guagliardi, A.; Burla, M. C.; Polidori, G.; Camalli, M. *J. Appl. Crystallogr.* **1994**, *27*, 435.
(37) Farrugia, L. J. *J. Appl. Crystallogr.* **1999**, *32*, 837.
(38) Sheldrick, G. M. *Acta Crystallogr., Sect. A* **1990**, *46*, 467.

TABLE 6. Crystallographic Data and Refinement Details for the Salts [1][NO_3]$_2$·2.5H_2O, [2][PF_6]$_2$, [3][PF_6]$_2$·2Me_2CO, [5][NO_3]$_2$·2MeCN, and [6][PF_6]$_2$·MeCN

	[1][NO_3]$_2$·2.5H_2O	[2][PF_6]$_2$	[3][PF_6]$_2$·2Me_2CO	[5][NO_3]$_2$·2MeCN	[6][PF_6]$_2$·MeCN
empirical formula	$C_{27}H_{29}N_8O_{8.5}$	$C_{30}H_{30}F_{12}N_6P_2$	$C_{40}H_{46}F_{12}N_6O_2P_2$	$C_{30}H_{27}N_7O_8$	$C_{34}H_{31}F_{12}N_5O_2P_2$
fw	601.58	764.54	932.77	613.59	831.58
cryst system	monoclinic	monoclinic	monoclinic	orthorhombic	orthorhombic
space group	$P2_1/c$	$P2_1/c$	$C2/c$	*Pnma*	*Pnma*
a/Å	19.223(1)	20.594(2)	20.603(7)	7.479(2)	8.050(1)
b/Å	10.223(1)	7.922(1)	23.48(1)	33.557(7)	39.19(1)
c/Å	13.931(1)	21.032(2)	8.922(3)	10.974(2)	11.293(2)
α/deg	90	90	90	90	90
β/deg	96.79(1)	112.424(4)	92.34(2)	90	90
γ/deg	90	90	90	90	90
V/Å^3	2718.5(3)	3171.8(6)	4313(3)	2754(1)	3562(1)
Z	4	4	4	4	4
T/K	100(2)	100(2)	100(2)	100(2)	100(2)
μ/mm^{-1}	0.112	0.242	0.196	0.110	0.226
cryst size/mm^3	0.30 × 0.10 × 0.03	0.20 × 0.10 × 0.08	0.30 × 0.10 × 0.05	0.65 × 0.15 × 0.05	0.25 × 0.20 × 0.05
appearance	dark red lath	dark red block	dark blue block	yellow plate	brown plate
no. of reflns collected	8464	9097	4112	9689	5666
no. of independent reflns (R_{int})	4730 (0.0516)	3815 (0.1347)	2148 (0.1082)	1275 (0.0783)	2199 (0.1025)
θ_{max}/deg (completeness)	25.03 (98.3%)	21.96 (98.4%)	20.81 (94.9%)	19.78 (99.9%)	21.95 (99.1%)
no. of reflns with $I > 2\sigma(I)$	2389	2351	1239	1061	1402
GOF on F^2	0.876	1.122	1.076	1.300	1.081
final R1, *w*R2 [$I > 2\sigma(I)$]	0.0582, 0.1272	0.1008, 0.1636	0.1182, 0.2811	0.0840, 0.1547	0.0966, 0.2203
final R1, *w*R2 (all data)	0.1207, 0.1440	0.1829, 0.2176	0.1863, 0.3247	0.1015, 0.1613	0.1350, 0.2354
peak and hole/eÅ^{-3}	0.824, −0.540	0.497, −0.354	0.555, −0.474	0.274, −0.405	0.490, −0.476

and refined by full-matrix least-squares on all F_0^2 data using SHELXL-97.[39] All non-hydrogen atoms were refined anisotropically and hydrogen atoms were included in idealized positions by using the riding model, with thermal parameters of 1.2 times those of aromatic parent carbon atoms, and 1.5 times those of methyl parent carbons. All other calculations were carried out with the SHELXTL package.[40] Crystallographic data and refinement details are presented in Table 6.

Hyper-Rayleigh Scattering. General details of the hyper-Rayleigh scattering (HRS) experiment have been discussed elsewhere,[18] and the experimental procedure and data analysis protocol for the fs measurements used in this study were as previously described.[19] Measurements were carried out in acetonitrile, with crystal violet as an external octupolar reference ($\beta_{xxx,800} = 338 \times 10^{-30}$ esu in methanol),[19a] and local field correction factors at optical frequencies were applied to correct for the difference in solvent. Measurements were performed by using the 800 or 880 nm output wavelengths of a regenerative, mode-locked Ti^{3+}:sapphire laser (Spectra Physics, model Tsunami, 100 fs pulses, 1 W, 80 MHz). Dilute solutions (10^{-4}−10^{-6} M) were used to ensure linear dependences of $I_{2\omega}/I_{\omega}^2$ on solute concentration, precluding the need for Lambert−Beer correction factors. The absence of frequency demodulation of the observed hyperpolarizability, i.e. constant values of β versus amplitude modulation frequency, showed that no fluorescence contributions to the HRS signals were present at 400 or 440 nm. This situation may indicate: (i) a lack of fluorescence, (ii) spectral filtering out of fluorescence, or (iii) the fluorescence lifetime is too short for its demodulation to be observed within the bandwidth of the instrument. The reported β values are the averages taken from measurements at different amplitude modulation frequencies. HRS depolarization ratios ρ[21] were determined at 800 or 880 nm in acetonitrile according to a published methodology.[41] While the precision of individual depolarization measurements is high (fitting errors of ca. ±0.02), multiple measurements on the crystal violet reference and on some of the samples indicated significant variability in the ρ values obtained. Hence the errors for the whole data set have been estimated based on the variability of ca. ±15% observed in the values obtained for the reference.

Stark Spectroscopy. The Stark apparatus, experimental methods, and data collection procedure were as previously reported,[25] except that a Xe arc lamp was used as the light source in the place of a W filament bulb. Butyronitrile was used as the glassing medium, for which the local field correction f_{int} is estimated as 1.33,[25] and the Stark spectrum for each compound was measured at least twice. Satisfactory fits of the Stark data for the salts [**1**][PF_6]$_2$ and [**4**][PF_6]$_2$ were obtained by using the observed absorption spectra, but for [**2**][PF_6]$_2$, [**3**][PF_6]$_2$, [**5**][PF_6]$_2$, and [**6**][PF_6]$_2$, these spectra were modeled with a sum of two or three Gaussian curves that reproduce the data and separate the peaks. The first and second derivatives of the Gaussian curves were then used to fit the Stark spectra with Liptay's equation.[26] The dipole-moment change, $\Delta\mu_{12} = \mu_e - \mu_g$, where μ_e and μ_g are the respective excited and ground-state dipole moments, associated with each of the curves considered in the fit was then calculated from the coefficient of the second derivative component. Note that the Gaussian fitting functions may not necessarily represent accurately individual electronic transitions, but are essential in order to allow the derivation of Stark data. Nevertheless, analyses of the combined data for the complete ICT bands are proven in this study and elsewhere[13k,14f,23,27] to afford physically sensible results and trends.

A two-state analysis of the ICT transitions gives

$$\Delta\mu_{ab}^2 = \Delta\mu_{12}^2 + 4\mu_{12}^2 \quad (4)$$

where $\Delta\mu_{ab}$ is the dipole-moment change between the diabatic states and $\Delta\mu_{12}$ is the observed (adiabatic) dipole-moment change. The value of μ_{12} can be determined from the oscillator strength f_{os} of the transition by

$$|\mu_{12}| = \left(\frac{f_{os}}{1.08 \times 10^{-5} E_{max}}\right)^{1/2} \quad (5)$$

where E_{max} is the energy of the ICT maximum (in wavenumbers) and μ_{12} is in eÅ. The latter is converted into Debye units upon

(39) Sheldrick, G. M. *SHELXL 97*, Program for Crystal Structure Analysis (Release 97−2); University of Göttingen: Göttingen, Germany, 1997.

(40) *SHELXTL*, Version 6.1; Bruker AXS Inc.; Madison: Wisconsin, 2000.

(41) (a) Hendrickx, E.; Boutton, C.; Clays, K.; Persoons, A.; van Es, S.; Biemans, T.; Meijer, B. *Chem. Phys. Lett.* **1997**, *270*, 241–244. (b) Boutton, C.; Clays, K.; Persoons, A.; Wada, T.; Sasabe, H. *Chem. Phys. Lett.* **1998**, *286*, 101–106.

multiplying by 4.803. The degree of delocalization c_b^2 and electronic coupling matrix element H_{ab} for the diabatic states are given by

$$c_b^2 = \frac{1}{2}\left[1 - \left(\frac{\Delta\mu_{12}^2}{\Delta\mu_{12}^2 + 4\mu_{12}^2}\right)^{1/2}\right] \quad (6)$$

$$|H_{ab}| = \left|\frac{E_{max}(\mu_{12})}{\Delta\mu_{ab}}\right| \quad (7)$$

If the hyperpolarizability β_0 tensor has only nonzero elements along the ICT direction, then this quantity is given by

$$\beta_0 = \frac{3\Delta\mu_{12}(\mu_{12})^2}{(E_{max})^2} \quad (8)$$

A relative error of ±20% is estimated for the β_0 values derived from the Stark data and using eq 8, while experimental errors of ±10% are estimated for μ_{12}, $\Delta\mu_{12}$, and $\Delta\mu_{ab}$, ±15% for H_{ab} and ±50% for c_b^2. Note that the ±20% uncertainty for the β_0 values is merely statistical and does not account for any errors introduced by two-state extrapolation.

Acknowledgment. We thank the EPSRC for support (grants EP/E000738 and EP/D070732) and also the Fund for Scientific Research-Flanders (FWO-V, G.0312.08), the University of Leuven (GOA/2006/3), and the NSF (grant CHE-0802907, Powering the Planet: an NSF Center for Chemical Innovation). I.A. is a postdoctoral fellow of the FWO-V. We thank Dr. Daniela Rusanova-Naydenova for obtaining some of the data presented in Figure 4, and are grateful to Dr Robin Pritchard of the University of Manchester for assistance with solving the crystal structure of salt [**2**][PF_6]$_2$.

Supporting Information Available: Crystallographic information in CIF format and ^{1}H and ^{13}C NMR spectra. This material is available free of charge via the Internet at http://pubs.acs.org.